Interactions between volcanism and geodynamics in the southern termination of the Ecuadorian arc

Mathilde Bablon, Xavier Quidelleur, Pablo Samaniego, Jean-Luc Le Pennec, Laurence Audin, Hervé Jomard, Stéphane Baize, Céline C. Liorzou, Silvana Hidalgo, Alexandra Alvarado

Tectonophysics 751 (2019) 54–72

Contents lists available at ScienceDirect

Tectonophysics

journal homepage: www.elsevier.com/locate/tecto

Interactions between volcanism and geodynamics in the southern termination of the Ecuadorian arc

Mathilde Bablon[a,*], Xavier Quidelleur[a], Pablo Samaniego[b], Jean-Luc Le Pennec[b,c], Laurence Audin[d], Hervé Jomard[e], Stéphane Baize[e], Céline Liorzou[f], Silvana Hidalgo[c], Alexandra Alvarado[c]

[a] GEOPS, Univ. Paris-Sud, CNRS, Université Paris-Saclay, 91405 Orsay, France
[b] Laboratoire Magmas et Volcans, Université Clermont Auvergne, CNRS, IRD, OPGC, F-63000 Clermont-Ferrand, France
[c] Instituto Geofísico, Escuela Politécnica Nacional, Ladrón de Guevara E11-253, Ap. 2759, Quito, Ecuador
[d] Institut des Sciences de la Terre, Université de Grenoble - IRD - CNRS, 1381 Rue de la piscine, 38400 Saint Martin d'Hères, France
[e] Institut de Radioprotection et de Sûreté Nucléaire, 31 Avenue de la Division Leclerc, 92260 Fontenay-aux-Roses, France
[f] Université de Bretagne Occidentale, Domaines Océaniques IUEM, 29280 Plouzané, France

ARTICLE INFO

Keywords:
Ecuador
K-Ar dating
Pallatanga fault
Volcanic arc migration
Slab flexure
Geodynamics

ABSTRACT

This study focuses on the construction and evolution through time of volcanic edifices located in the southern part of the Ecuadorian arc, with the objective to contribute to a better understanding of the interactions between magmatism, slab geometry and the activity of tectonic faults. Our new groundmass K-Ar ages obtained for a dozen volcanoes from the southern Quaternary arc are rather young, without ages older than 800 ka, and highlight an increasing volcanic activity between 300 and 100 ka. These new temporal constraints suggest that a southward migration of the Ecuadorian arc occurred during the last 600 ka. We interpret this evolution as the result of major and recent geodynamic reorganization in Ecuador related to the activation of lithospheric faults and to the flexure of the slab at depth, following the inland prolongation of the Grijalva fracture zone. Both phenomena could have been induced by the oblique subduction of the Nazca plate towards the convex margin of the South American continent, and the coupling of these two plates along the Wadati-Benioff zone, progressively intensified by the Carnegie ridge subduction. Southward migration of the slab flexure at depth could have changed pressure and temperature conditions, favoring the partial melting of the mantle wedge and magma genesis, thereby inducing a southward migration of the Ecuadorian arc volcanoes. These results contribute therefore to a better knowledge of the current arc dynamics in the Northern Andes, and provide insights into the use of geochronological data applied to volcanic rocks for studies of past tectonic activity in Ecuador.

1. Introduction

The geodynamic setting of continental Ecuador is characterized by a considerable volcanic activity since the Pleistocene, with more than 80 volcanoes active during the Quaternary, including 25 active during the Holocene (e.g., Barberi et al., 1988; Hall and Beate, 1991; Hall et al., 2008; Bernard and Andrade, 2011). Eight of these volcanic edifices are considered still active, namely with their latest activity during the so-called historical time (i.e. younger than 500 years BP). Four of them have been active during the last few years: Reventador, Cotopaxi, Tungurahua and Sangay volcanoes (www.igepn.edu.ec). The Ecuadorian volcanic arc originates from the subduction of the oceanic Nazca plate beneath the South American continent (Fig. 1a). The volcanic front position is intimately linked to the geometry at depth of the subducting plate (e.g., Tatsumi, 1986; Guillier et al., 2001; Syracuse and Abers, 2006), which in turn is controlled by the structures of the subducted slab and the convexity of the Ecuadorian margin. Among these structures, we can mention the Carnegie ridge, which is the trace of the Galápagos hotspot activity on the Nazca plate, as well as the Grijalva fracture zone, an escarpment separating two oceanic crust segments of different ages, older than 30 Ma south and younger than 20 Ma north of the fracture zone (Lonsdale, 2005). As recently pointed out by Yepes et al. (2016), these features induce a flexure of the slab under the Quaternary volcanic arc. Consequently, the slab dips at an angle of ~22° north of the Carnegie ridge, while the dip is more pronounced below the southern termination of the arc (30–35°), then

* Corresponding author.
E-mail address: mathilde.bablon@u-psud.fr (M. Bablon).

https://doi.org/10.1016/j.tecto.2018.12.010
Received 9 May 2018; Received in revised form 10 December 2018; Accepted 11 December 2018
Available online 17 December 2018
0040-1951/

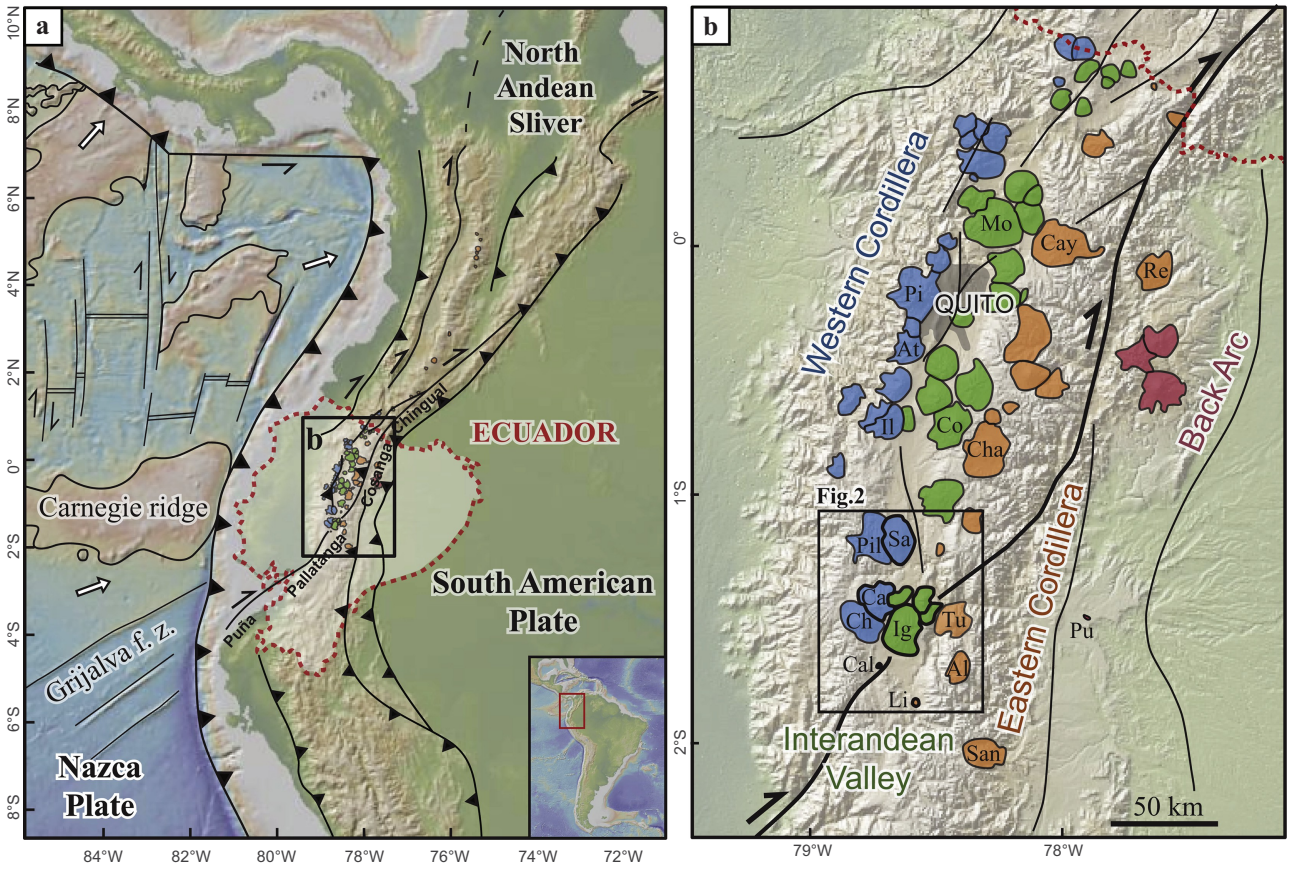

Fig. 1. a) Geodynamic and tectonic setting of the Northern Volcanic Zone of the Andes. The topography map is modified from GeoMapApp, which uses data of Smith and Sandwell (1997). Borders of Ecuador are represented with orange dotted lines. White arrows indicate the direction of plate motion relative to South America (DeMets et al., 2010). Main faults and tectonic structures are represented by the black lines, modified from Tibaldi et al. (2007), Baize et al. (2015) and Alvarado et al. (2016). b) Map of the Ecuadorian arc (modified from Hall et al., 2008), comprising volcanic edifices distributed along the Western Cordillera (blue), the Interandean Valley (green), the Eastern Cordillera (orange) and the Back Arc (red). Quito, the capital city, is represented in grey. Black lines represent the location of the main faults, and the thick line corresponds to the Chingual-Cosanga-Pallatanga-Puña (CCPP) fault. The studied volcanoes are drawn with heavy black borders. Al: Altar; At: Atacazo; Ca: Carihuairazo; Cal: Calpi cones; Cay: Cayambe; Ch: Chimborazo; Cha: Chalupas; Co: Cotopaxi; Ig: Igualata; Il:Iliniza; Li: Licto cone; Mo: Mojanda; Pi: Pichincha; Pil: Pilisurco; Pu: Puyo cones; Re: Reventador; Sa: Sagoatoa; San: Sangay; Tu: Tungurahua. (For interpretation of the references to colour in this figure legend, the reader is referred to the web version of this article.)

significantly decrease south of the Grijalva fracture zone, with an angle of 12° (Yepes et al., 2016). In addition, this part of the Andean chain has a large number of active crustal faults, notably along the Chingual-Cosanga-Pallatanga-Puná fault system (e.g., Baize et al., 2015; Alvarado et al., 2016; Fig. 1a), mainly related to the oblique subduction of the Nazca plate. Consequently, combined seismic and volcanic hazards in Ecuador are a high threat for both local populations and infrastructure. The Ecuadorian volcanic arc is, therefore, particularly suitable for the investigation of interactions between geodynamics, tectonics and volcanism. Despite a thorough investigation of kinematics along crustal faults (e.g., Winter et al., 1993; Lavenu et al., 1995; Ego et al., 1996; Tibaldi et al., 2007; Alvarado et al., 2014; Baize et al., 2015; Alvarado et al., 2016; Champenois et al., 2017), few Quaternary data with accurate timing control are available for fault activity prior to the Holocene. On the other hand, focused geochronological data are available for several volcanic edifices, such as Cayambe (Samaniego et al., 2005), Chacana (Opdyke et al., 2006), Atacazo-Ninahuilca (Hidalgo, 2006; Hidalgo et al., 2008), Pichincha (Robin et al., 2010), Imbabura (Le Pennec et al., 2011), Chimborazo (Samaniego et al., 2012), Chachimbiro (Bernard et al., 2014), Antisana (Hall et al., 2017) and Tungurahua volcanoes (e.g., Hall et al., 1999; Le Pennec et al., 2013; Bablon et al., 2018a). Although some studies also focused on the development of the Ecuadorian arc at a more regional scale (e.g., Hall and Wood, 1985; Barberi et al., 1988; Hall and Beate, 1991; Opdyke et al., 2006), the overall chronology of the arc development is still poorly documented.

The present study combines new geochronological data of volcanic activity and mapping of the main faults in the southern termination of the Ecuadorian arc (Monzier et al., 1999a), where numerous volcanic edifices and active faults appear to have been concomitant or influencing each other. This work aims to examine the potential influence of the geodynamics on the arc development, and to contribute to a better understanding of the large increase of volcanic activity in Ecuador during the Quaternary.

2. Geological and geodynamical context of the Ecuadorian arc

2.1. Orogeny and tectonics of the Ecuadorian Andes

The subduction of the former oceanic Farallón plate beneath the continental South American lithosphere began during the Late Triassic - Early Jurassic period (James, 1971; Aspden et al., 1987). Between ca. 75 and 55 Ma, oceanic terranes were accreted to the Ecuadorian and Colombian margins in several tectonic episodes (e.g., Spikings et al., 2001; Kerr et al., 2002; Hughes and Pilatasig, 2002; Jaillard et al., 2008; Jaillard et al., 2009). The current Andean range originates from the subduction of the Nazca plate, formed after the breakup of the older Farallón plate between 23 and 27 Ma, related to the activity of the Galápagos spreading center (Hey, 1977; Lonsdale and Klitgord, 1978;

Pennington, 1981; Meschede and Barckhausen, 2001; Sallarès and Charvis, 2003; Lonsdale, 2005).

The width of the Quaternary volcanic arc ranges between ~60 and 150 km in front of the Carnegie Ridge (Fig. 1a), and the volcanoes are distributed north of 2°S in Ecuador. They mostly lie to the north of the inland prolongation of the Grijalva fracture zone, located roughly below Chimborazo and Carihuairazo-Puñalica volcanoes (Fig. 1b). However, some edifices from the southern termination of the arc, such as Sangay, Altar, Igualata and Tungurahua volcanoes, as well as Puyo, Calpi and Licto cones, are located south of the inland prolongation of the Grijalva fracture zone (Yepes et al., 2016; Ancellin et al., 2017; Narvaez et al., 2018). Ecuadorian volcanoes are distributed in the Western and Eastern Cordilleras, the Interandean Valley and the back-arc area (e.g., Hall and Beate, 1991; Hall et al., 2008). The volcanic front of the Western Cordillera is mainly composed of andesitic to dacitic compound stratovolcanoes, while the intermediate arc, including the Interandean Valley and the Eastern Cordillera is mostly made up of andesitic stratovolcanoes. The calc-alkaline magmatic series of these volcanoes contrasts with the alkaline products emitted from back-arc edifices (e.g., Hall et al., 2008; Fig. 1b). The basement of the Western Cordillera and the western part of the Interandean Valley is composed of accreted oceanic terranes (e.g., Jaillard et al., 2009; Fig. 1b), whereas the Eastern Cordillera basement is made up of Paleozoic to Mesozoic plutonic and metamorphic rocks with a mostly continental affinity. Lastly, the back-arc is composed of late Cretaceous sedimentary deposits, which overlie Paleozoic-Lower Cretaceous metamorphic rocks and the continental Precambrian craton (Coltorti and Ollier, 2000; Barragán et al., 2005; Hall et al., 2008). Moreover, the fast (~6 cm·a^{-1}; Trenkamp et al., 2002; Kendrick et al., 2003; Nocquet et al., 2014) and oblique (~N81°E; Kendrick et al., 2003; Bird, 2003; DeMets et al., 2010; Nocquet et al., 2014) subduction of the Nazca plate, combined with the subduction of the Carnegie Ridge (Pennington, 1981; Gutscher et al., 1999; Witt et al., 2006; Fig. 1a), produce a displacement of the northwestern part of the South America continent (e.g., Egbue and Kellogg, 2010; Nocquet et al., 2014). This domain, previously called the "Andean Block" (Pennington, 1981; Ego et al., 1996), and then the "North Andean Block" (Kellogg and Vega, 1995; Witt et al., 2006; Alvarado et al., 2014), has been recently introduced as "North Andean Sliver" (Nocquet et al., 2014; Alvarado et al., 2016; Fig. 1a) in order to properly depict the internal crustal deformation of the block inferred from geodesy. Paleoseismological, geodetic and field studies propose that the deformation generated by this displacement is accommodated along a mature dextral strike-slip fault zone, called the Chingual-Cosanga-Pallatanga-Puná (CCPP) fault system (Baize et al., 2015; Alvarado et al., 2016; Fig. 1a and b), with a current geodetic bulk velocity of ~8 mm·a^{-1} (Nocquet et al., 2014). This fault system extends from the Gulf of Guayaquil to the Caribbean Sea, and roughly corresponds to the previous Dolores-Guayaquil Megashear (e.g., Lavenu et al., 1995). In Ecuador, it crosses the Western Cordillera between ~2°S and ~1.7°S (Fig. 1a), the Interandean Valley around ~1.5°S, through Igualata volcano (Fig. 1b), then goes along the Eastern Cordillera north of 1°S. The onset of activity of the CCPP fault is still debated but seems to have occurred during the Pliocene - Early Pleistocene (Lavenu et al., 1995). Indeed, offshore sedimentary records indicate that the opening phase and high sedimentation rate of the Gulf of Guayaquil occurred during the Early Pleistocene (Deniaud et al., 1999; Witt et al., 2006), while the Miocene fore-arc marine basins were uplifted during the Pliocene and filled up with continental deposits during the Pleistocene (Spikings et al., 2001; Alvarado et al., 2016). Local sections of this fault were studied onshore (Winter et al., 1993; Lavenu et al., 1995; Dumont et al., 2005; Tibaldi et al., 2007; Alvarado et al., 2014; Baize et al., 2015; Champenois et al., 2017), and ^{14}C dating revealed that the fault system has been continuously active during the Holocene, with an average slip rate of 2.5 to 5 mm·a^{-1} for the Pallatanga fault segment (Winter et al., 1993; Baize et al., 2015). Finally, the collision age of the Carnegie Ridge (Pennington, 1981; Gutscher et al., 1999; Witt et al., 2006; Fig. 1a) to the Ecuadorian margin is still debated and ranges between 1 and 15 Ma (e.g., Lonsdale and Klitgord, 1978; Gutscher et al., 1999; Spikings et al., 2001). However, many evidences suggest that the collision occurred during the last 5 Ma, such as paleogeographic reconstructions (Collot et al., 2009), sedimentation rates of the Gulf of Guayaquil (Deniaud et al., 1999; Witt et al., 2006), the uplift of the margin and basins (e.g. Gutscher et al., 1999; Graindorge et al., 2004; Pedoja et al., 2006), as well as the volcanism distribution and geochemistry (e.g., Hall and Wood, 1985; Barberi et al., 1988; Samaniego et al., 2010).

2.2. Geological context of the southern termination of the Ecuadorian arc

The southern termination of the Ecuadorian arc is composed of a dozen volcanic edifices, active during the Plio-Quaternary (Hall and Wood, 1985; Barberi et al., 1988; Hall and Beate, 1991; Hall et al., 2008). This group of volcanoes is separated from the central and northern part of the arc by a 50–100 km-long gap without active volcanism. A review of the previously published data for these edifices is presented below, from the Western to the Eastern Cordillera.

Sagoatoa volcano (4169 m above sea level (a.s.l.); Lat. 01°09′S; Long. 78°04′W) is located north of our study area, on the western edge of the Interandean Valley. This volcano is part of a large complex, with Pilisurco volcano (4508 m; Fig. 1b) located to the west. The erosion having affected its flanks appears important, with smooth surfaces incised by deep valleys. Two K-Ar ages have been published, at 1.73 ± 0.35 and 1.40 ± 0.29 Ma (Lavenu et al., 1992). Nevertheless, these ages should be considered with caution as they were carried out on plagioclases and whole-rock, respectively, which, hence, may include phenocrysts containing inherited radiogenic argon and/or weathered areas, possibly leading to erroneously old ages (e.g., Harford et al., 2002; Samper et al., 2008).

South of Sagoatoa, the activity of ***Carihuairazo*** volcano (5018 m a.s.l.; Lat. 01°24′S; Long. 78°45′W) began at least ~225 ka (Samaniego et al., 2012). In the Ambato basin, northeast of the volcano (Fig. 2a), four sequences of sector collapse and block-and-ash deposits are interbedded with plinian fallout deposits from Huisla volcano. The debris avalanche deposits (DAD) of Carihuairazo located at the base of the sequence are older than 45 ka; the second sector collapse occurred before ~40 ka; and the more recent tephra fallout and debris avalanche deposits, which cover the sequence, are younger than ~40 ka based on uncalibrated ^{14}C age determinations (Clapperton, 1990; Ordóñez, 2012). Moreover, these deposit sequences cover the deposits of the Chalupas ignimbrite, a major Ecuadorian stratigraphic marker dated at ~215 ka (Beate et al., 2006; Bablon et al., 2018b). Volcanic activity of Carihuairazo ended with the growth of several domes on its eastern flank (Ordóñez, 2012).

Puñalica (3988 m a.s.l.; Lat. 01°24′S; Long. 78°41′W; Fig. 2a), a morphologically fresh-looking edifice, is located on the northeast flank of Carihuairazo volcano, and may correspond to its last volcanic activity (Clapperton, 1990). Puñalica is made up of basic volcanic products that cover the older moraines of the Last Glacial Maximum (LGM), but do not crop out on the youngest ones, which suggests that some parts of the volcano were constructed between 14 and 18 ka (Clapperton, 1990).

Further south, the activity of ***Chimborazo*** volcano (6268 m a.s.l.; Lat. 01°28′S; Long. 78°49′W) began at ~120 ka, and is considered still active (Clapperton, 1990; Barba et al., 2008; Bernard et al., 2008; Samaniego et al., 2012). The volcano is composed of three successive edifices, and experienced a major sector collapse at the end of Chimborazo I construction, at ~60–65 ka (Samaniego et al., 2012). The debris avalanche deposit spread out into the Riobamba basin (Fig. 2d), incorporating older deposits of the Chalupas ignimbrite. The Guano lava flow, in the northern edge of the basin (Fig. 2d), corresponds to volcanic products erupted after the sector collapse, as it locally overlies the avalanche deposit. The proximal outcrops of this debris avalanche deposit are covered by LGM moraines, suggesting that both the Guano

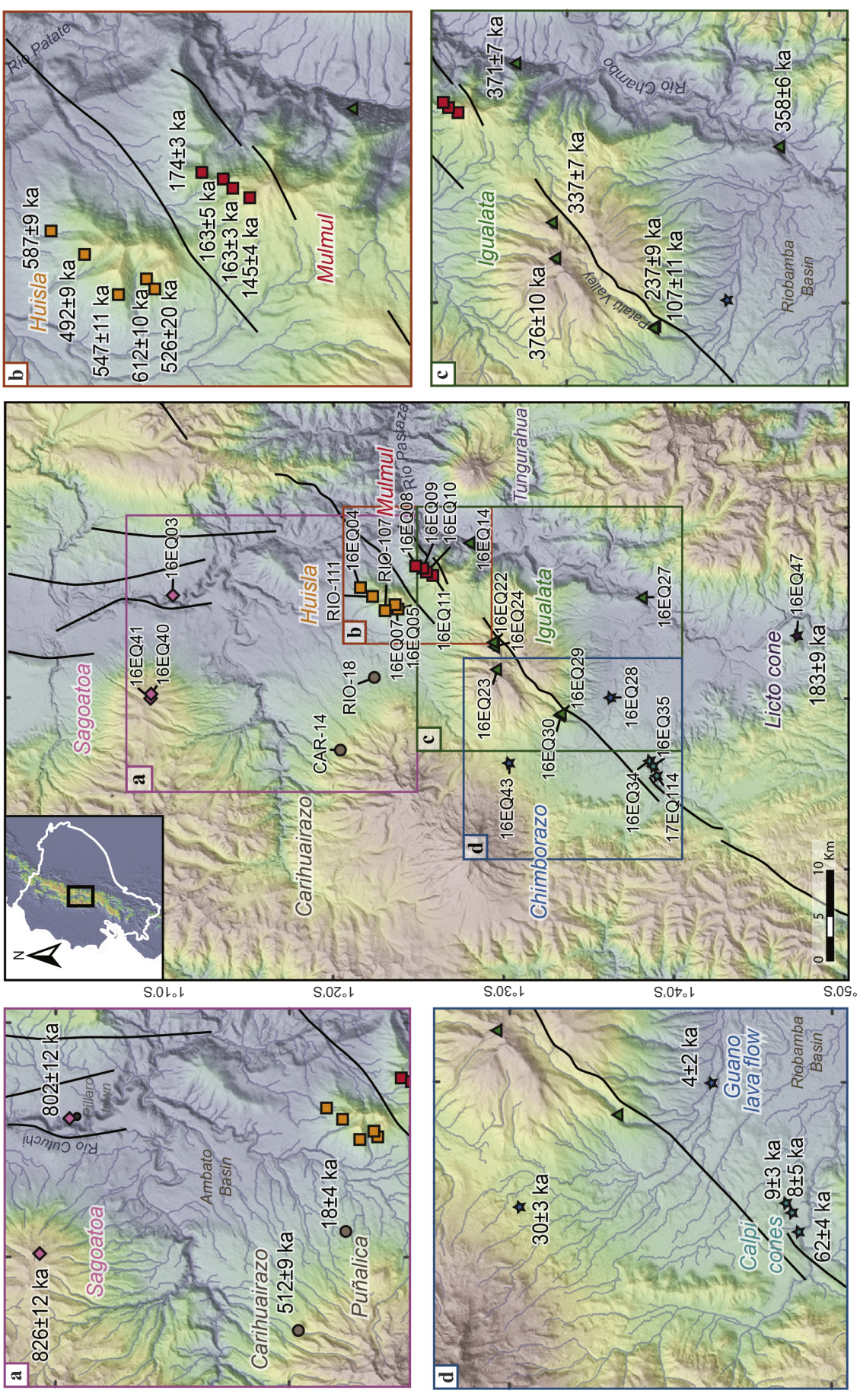

Fig. 2. Shaded view of the Digital Elevation Model (DEM; 30-m resolution) of the studied area showing samples location and number. Blue lines represent the main rivers, and black lines indicate the location of the Pallatanga fault segments, described in detail in Baize et al. (2016). a), b), c), and d) are focus views of Sagoatoa and Carihuairazo volcanoes, Huisla and Mulmul volcanoes, the Riobamba basin, and Igualata volcano, respectively, including our new K-Ar ages location. (For interpretation of the references to colour in this figure legend, the reader is referred to the web version of this article.)

lava flow and the sector collapse are older than 33 ka (Samaniego et al., 2012). Moreover, ash flow deposits from Chimborazo II dated at ~43 ka also cover the sector collapse deposits, implying that the latter is older than 43 ka (Samaniego et al., 2012).

Located on the western edge of the Interandean Valley, northwest of Tungurahua volcano (Fig. 1b), ***Huisla*** volcano (3763 m a.s.l.; Lat. 01°24′S; Long. 78°34′W) is an andesitic edifice, previously called Cerro Llimpi (Stübel, 1897). On the basis of isopach maps and geochemistry, at least three tephra fallout deposits, exposed in the Ambato basin, northwest of the volcano (Fig. 2), have been assigned to Huisla (Ordóñez, 2012). The two younger plinian eruptions occurred in the last 39 ka (Ordóñez, 2012). This edifice experienced a sector collapse of its southeastern flank (Espín et al., 2018), whose resulting debris avalanche deposits cover the Chalupas ignimbrite (Bustillos, 2008; Espín, 2014). However, no geochronological data from lava flows are available for this volcano, nor for the surrounding volcanic edifices, such as ***Mulmul*** (3878 m a.s.l.; Lat. 01°26′S; Long. 78°33′W) and ***Igualata*** (4430 m a.s.l.; Lat. 01°30′S; Long. 78°38′W) volcanoes.

The volcanic arc in the Interandean Valley ends to the south with the ***Calpi*** and ***Licto scoria cones***, in the southern edge of the Riobamba basin (Fig. 2d). Only geochemical data are available for these edifices (Ancellin et al., 2017); their periods of activity are still unknown but stratigraphic evidences point out to an age older than the debris avalanche deposit of Chimborazo volcano (Bernard et al., 2008; Clapperton, 1990).

In the Eastern Cordillera, only ***Tungurahua*** volcano (Fig. 1b) was studied in detail. (e.g., Hall et al., 1999; Le Pennec et al., 2006; Bablon et al., 2018a). Its activity began at ~300 ka, and the volcano was erupting between 1999 and 2016. Made up of three successive edifices, it experienced two major sector collapses, at ~35 and ~3 ka (Hall et al., 1999; Le Pennec et al., 2013). In the Río Chambo valley, southwest of the volcano, the oldest avalanche deposit covers another avalanche deposit originated from ***Altar*** volcano (Bustillos, 2008). However, the period of activity of the latter remains undocumented.

The construction of ***Sangay*** volcano, the southernmost active volcano of the arc, began at ~500–400 ka (Monzier et al., 1999b). This mainly andesitic stratovolcano is made up of three edifices and experienced two undated major flank collapses (Valverde, 2014).

Finally, the ***Puyo cones***, made up of alkali basalts, were emplaced in the back-arc around 200 ka (Hoffer et al., 2008).

In this study, we present twenty-four new K-Ar ages on groundmass, and their corresponding major and trace element contents, performed on lava flows from eight different volcanoes (Huisla, Mulmul, Igualata, Carihuairazo, Chimborazo, Sagoatoa, as well as Licto and Calpi cones; Fig. 1b), to investigate the temporal evolution of the southern termination of the Ecuadorian arc.

3. Materials and methods

3.1. Rock sampling for K-Ar dating and geochemical analyses

Twenty-six lava flows were sampled from several edifices (Fig. 2), mostly located between Chimborazo and Tungurahua volcanoes (Fig. 1b). Whenever possible, we sampled outcrops located in the deep incised valleys and in the summit area of the edifices, in order to determine their whole period of activity.

Three lava flows were sampled from ***Sagoatoa*** volcano. Sample 16EQ03 is from a distal lava flow located in the Río Cutuchi valley, northwest of Píllaro town (Fig. 2a). This lava flow is covered by the Chalupas ignimbrite, while samples 16EQ40 and 16EQ41 are located near the summit of the volcano.

We sampled proximal (16EQ43) and distal (16EQ28) areas of the ***Guano lava flow*** (Fig. 2d), which originated from Chimborazo volcano (Samaniego et al., 2012), and followed the southern flank of Igualata, north of the Riobamba basin. As this lava flow is cut and slightly shifted by the Pallatanga fault (Baize et al., 2016), its age might bring valuable insights regarding the period of activity and the velocity of the fault displacement.

Two lava flows were sampled in order to constrain the timing of the construction of ***Carihuairazo*** volcano. Sample CAR-14 (Fig. 2a) is from ***Tzunantza dome*** (also spelled Cerro Sunantza; Ordóñez, 2012), located at the foot of its northern flank, while RIO-14 is from the young ***Puñalica*** edifice.

The morphology of ***Igualata*** (Fig. 2d) is rather similar to that of Sagoatoa volcano, except for its large *E*-W trending summit depression. This depression is similar to a pull-apart structure controlled by the NE-SW dextral Pallatanga fault. Samples 16EQ22 and 16EQ24 are from lava flows interbedded with breccia layers, in the upper part of the northern flank, north of this structure. Sample 16EQ23 is from a lava flow located at the summit of the volcano. Because of agricultural fields and abundant vegetation present in the southern flank, we only sampled two rocks, in the Patalú valley, which drains the southwest flank of Igualata volcano down to the Riobamba basin (Fig. 2d). Sample 16EQ30 is from a juvenile block from a ~10 m-thick block-and-ash flow deposit, which covers an older lava flow (sample 16EQ29), located at the bottom of the valley.

Two basal lava flows were also sampled in the Río Chambo valley, at the foothill of Mulmul (l6EQ14) and Igualata (16EQ27) volcanoes (Fig. 2). They are mapped as deposits from the Mio-Pliocene Pisayambo formation (Litherland et al., 1993; Hughes and Pilatasig, 2002), and may represent an old and extinct volcanic activity. The outcrop of 16EQ27, more than 150 m-wide, presents tilted blocks, several dykes and numerous vesiculated enclaves with a phaneritic texture made up of plagioclase and amphibole phenocrysts (see Appendix A for photographs of thin sections).

Five lava flows were sampled in basal areas or in deep incised valleys on northern (16EQ04, RIO-111) and western (RIO-107, 16EQ05, 16EQ07) flanks of ***Huisla*** volcano (Fig. 2b). Unfortunately, no lava from the terminal activity crops out at the summit of this edifice. We sampled four lava flows from ***Mulmul*** volcano (Fig. 2b), which partly grew in the collapse amphitheater of Huisla volcano. Sample 16EQ08 is from a monogenetic breccia deposit containing juvenile blocks included in an ash-rich matrix, which was probably related to a dome collapse, while samples 16EQ09, 16EQ10 and 16EQ11 are from lava flows from the northwestern flank.

Finally, three cones located in the Riobamba basin were sampled (Fig. 2). Samples 16EQ34, 16EQ35 and 17EQ114 are from slightly vesicular lava flows from ***Calpi cones***, located along the Pallatanga fault, north-west of Riobamba city. The two former correspond to proximal lava flows, while 17EQ114 is a distal lava flow covered by the debris avalanche deposits of Chimborazo volcano. Sample 16EQ47, located in the southernmost part of our study area, is from a lava flow from ***Licto cone*** (Cerro Tulabug), which is covered by varved lacustrine deposits associated with the distal parts of the Chimborazo DAD.

The freshest samples, selected after a careful examination of thin sections (Appendix A), were dated by the potassium-argon (K-Ar) dating method applied to the groundmass, while the whole-rock major and trace element contents were measured for all samples.

3.2. K-Ar dating method and protocol

The K-Ar dating method was applied to the groundmass, using the unspiked Cassignol-Gillot technique (Cassignol and Gillot, 1982). This technique was developed for Quaternary volcanoes, whose lavas contain low radiogenic argon ($^{40}Ar^{*}$; Gillot et al., 2006). It has been shown to be particularly suitable for dating young calk-alkaline lavas, such as in Ecuador for Tungurahua volcano (Bablon et al., 2018a), as well as in Argentina or in the Lesser Antilles (Samper et al., 2009; Germa et al., 2010; Germa et al., 2011; Ricci et al., 2015). The description of sample preparation and analytical procedures, standards used and uncertainty calculations are given in Bablon et al. (2018a). Samples were crushed and sieved to 63–80, 80–125 or 125–250 μm, based on the size of the

phenocrysts, which must be removed, and on the groundmass proportion. The technique relies on the detection of the very small difference between the isotopic $^{40}Ar/^{36}Ar$ ratio of the groundmass extracted from the sample and the atmospheric ratio. The result corresponds to the quantity of $^{40}Ar^{*}$ produced by the radioactive decay of ^{40}K since the eruption. Therefore, together with the potassium content of the groundmass and the ^{40}K decay constants (Steiger and Jäger, 1977), we can calculate the age of the lava sample. Both potassium and argon measurements were carried out at the GEOPS laboratory in Orsay (Paris-Sud University, France). All measurements were performed at least twice in order to check their reproducibility within uncertainty, except for samples 16EQ28, 16EQ34 and 16EQ35, for which the argon content was measured five times, in order to improve the precision calculated for the mean age. As the five ages obtained for each aliquot are consistent within uncertainty, we can calculate the mean age by averaging each analysis, weighted by the inverse of its variance. The final age uncertainty of these three samples is obtained as the reciprocal square root of the five reciprocal variances sum (Taylor, 1997). Ages reported throughout this study are given at the 1-σ confidence level.

3.3. Geochemical analyses

The analytical procedure for measurement of major and trace element content is detailed in Cotten et al. (1995). Agate-crushed powders of the twenty-three whole-rock samples were analyzed by ICP-AES (Inductively Coupled Plasma - Atomic Emission Spectrometry), at the LGO (Laboratoire Géosciences Océan) of the Université de Bretagne Occidentale (Brest, France). Relative uncertainties are lower than 2% and 5%, for major and trace elements, respectively. Major element concentrations were recalculated to a total of 100% on a water free-basis. Major and trace element concentrations are given in Table 2.

4. Results

4.1. K-Ar groundmass dating

Twenty-five K-Ar ages obtained in this study is presented in Table 1 and Fig. 2. All samples have porphyritic textures with a variable amount of plagioclase, ortho- and clinopyroxene, Fe-Ti oxides, olivine, and amphibole phenocrysts (Appendix A). Overall, the groundmass represents about up to 50% of the rocks, and generally contains microlites of plagioclase, pyroxene and Fe-Ti oxides into a glassy matrix. The K content of the separated groundmass ranges between 1.3 and 3.1 wt%, and radiogenic argon content ranges between 0.04% and 24.88%. The mean density of the dated fractions is about 2.66 $g{\cdot}cm^{-3}$. The ages obtained for each edifice are detailed below, from the Western to the Eastern Cordillera.

Both samples from ***Sagoatoa*** volcano have similar ages: 826 ± 12 ka for the summit (16EQ40), and 799 ± 12 ka for the eastern distal lava flow (16EQ03; Fig. 2a). These ages probably represent the terminal activity of the volcano, and, although we do not have any lava flow from its initial stages, Sagoatoa volcano is the oldest edifice of our study.

Further south, the sample from Tzunantza dome (CAR-14; Fig. 2a), to the north of ***Carihuairazo*** volcano, is dated at 512 ± 9 ka. Given that Carihuairazo lavas have been dated at ~225 ka by Samaniego et al. (2012), this age may correspond to an older, pre-Carihuairazo activity. The volcanic activity around Carihuairazo area may have ended with the formation of ***Puñalica*** edifice, at 18 ± 3 ka (RIO-18).

Guano lava flow unit samples, related to the post-collapse activity of Chimborazo, show two significantly different ages, which indicate that the proximal and distal areas do not belong to a single lava flow. Indeed, the proximal sample yields 30 ± 3 ka (16EQ43), while the distal sample suggests the existence of a Holocene lava flow emission from Chimborazo volcano, with an age of 4 ± 2 ka (16EQ28; Fig. 2c).

In the Interandean Valley, ***Igualata*** volcano seems to be older than the neighboring volcanoes, based on the high erosion of its flanks and its morphology. However, the oldest sample is dated at 376 ± 10 ka (16EQ23; Fig. 2d), although we could not sample the base of this edifice, due to the lack of outcrops. On the southwestern flank, the lava flow located in the valley incised along the Pallatanga fault is dated at 237 ± 9 ka, while the pyroclastic flow deposit sequence, dated at 107 ± 11 ka (Fig. 2d), is the most recent outcrop dated from this volcano. Eastward, the two lava flows sampled as basement lavas yielded ages of 358 ± 6 and 371 ± 7 ka, for sample 16EQ27 located south of Igualata volcano, and for sample 16EQ14 located on the eastern foot of Mulmul volcano, respectively. Both ages are too young to be associated with the old volcanic basement (Litherland et al., 1993; Hughes and Pilatasig, 2002), and they are in the same range as those obtained for Igualata volcano, with a similar geochemical composition (see below). Thus, these lava flows should be related to the base of this edifice.

Huisla volcano appears older than Igualata and coeval with Tzunantza dome, north of Carihuairazo, with five ages ranging between 612 ± 10 ka (16EQ07) and 492 ± 9 ka (RIO-111; Fig. 2b). The ages obtained for ***Mulmul*** volcano are consistent with the fact that it partly grew within the sector collapse amphitheater of Huisla volcano. Indeed, ages are younger than those of Huisla, and range between 174 ± 3 ka (16EQ08) and 145 ± 4 ka (16EQ11; Fig. 2b).

Finally, the timing of construction of ***Licto*** and ***Calpi cones***, within the Riobamba basin, is significantly different. In fact, the lava flow of Licto cone is dated at 183 ± 9 ka (16EQ47), while the proximal lava flows of Calpi monogenic cones display ages of 9 ± 3 and 8 ± 5 ka (16EQ34 and 16EQ35, respectively; Fig. 2c). The distal lava flow of Calpi (17EQ114), covered by the debris avalanche deposits of Chimborazo, was emitted at 62 ± 4 ka. Consequently, Calpi cones could have been constructed in at least two stages. The oldest stage occurred before the major sector collapse event of Chimborazo volcano (Clapperton, 1990; Bernard et al., 2008; Samaniego et al., 2012), and the youngest stage corresponds to the construction of the cones during the Holocene. Detailed field investigations on this part are needed in order to better support this hypothesis.

4.2. Whole rock geochemical analyses

Geochemical analyses of the twenty-seven samples show that they belong to the medium-K calc-alkaline series in the K_2O vs. SiO_2 diagram (Peccerillo and Taylor, 1976; Fig. 3a). Sample RIO-111, from ***Huisla*** volcano, plots in the limit between the medium and high-K calc-alkaline series. Silica contents range between 52.8 and 65.9 wt%, and K_2O content between 1.5 and 2.6 wt%. Hence, lavas from this study are mainly basaltic andesites and andesites, with some dacitic rocks, such as the youngest lava flow of Huisla (RIO-111), the lava flow at the summit of ***Sagoatoa*** (16EQ40), and the pyroclastic flow deposit of ***Igualata*** volcano (16EQ30; Fig. 3a). The ***Licto cone*** lava flow is a basaltic andesite, as well as those from ***Puñalica*** (RIO-18) and from the southern ***Calpi cone*** (16EQ35), while other samples from Calpi cones (16EQ34 and 17EQ114) are andesitic lavas with silica content of ~61%. All samples from Huisla volcano plot in the field of both in-situ lava flows and blocks of the collapse deposits (Bustillos, 2008; Fig. 3a). Finally, we note that most samples have lower potassium content than Tungurahua lava flows (Fig. 3a), located in the Eastern Cordillera. Indeed, the content of most of the incompatible elements, including K, increases with the distance from the trench, interpreted as a lower degree of mantle partial melting (Barragán et al., 1998; Hidalgo et al., 2012; Ancellin et al., 2017).

Spider diagrams of trace elements normalized to the primitive mantle, and diagrams of Rare Earth Elements (REE) normalized to chondrites (Sun and McDonough, 1989; Fig. 3b and c), show enrichment of Large-Ion Lithophile Elements (LILE; Rb, Ba, and K) and Light REE (LREE; La, Ce, Nd), as well as a depletion of High-Field Strength Elements (HFSE; Nb, Ti and Y). These patterns are typical of arc

Table 1
New groundmass K-Ar ages obtained in this study. Column headings indicate sample name, detail of the outcrop location, sample coordinates projected using the Universal Transverse Mercator (UTM) coordinate system (Zone 17), potassium concentration in percent, radiogenic argon content in percent, and in atoms per gram ($\times 10^{11}$), ages, and weighted mean age in ka, with 1-sigma uncertainty. Ages marked with an asterisk (*) were calculated using reciprocal variances weighted average (see text).

Sample	Location	Longitude (m)	Latitude (m)	K (%)	$^{40}Ar^{*}$ (%)	$^{40}Ar^{*} \times 10^{11}$ (at/g)	Age ± 1σ (ka)	Mean age (ka)
Sagoatoa volcano								
16EQ40	Lava flow, summit	759,889	9,872,238	2.512	22.10	21.661	825 ± 12	826 ± 12
					19.66	21.721	828 ± 12	
16EQ03	Distal lava flow, west of Píllaro city	770,638	9,869,872	1.639	24.88	13.710	801 ± 12	799 ± 12
					22.84	13.651	797 ± 12	
Carihuairazo volcano								
CAR-14	Tzunantza dome, N flank	753,880	9,851,817	1.287	8.46	6.9239	515 ± 9	512 ± 9
					10.58	6.8446	509 ± 9	
RIO-18	Distal lava flow from Cerro Puñalica	761,709	9,848,098	1.409	0.59	0.2953	20 ± 3	18 ± 3
					0.52	0.2357	16 ± 3	
Chimborazo volcano								
16EQ43	Proximal deposit of Guano lava flow	752,451	9,833,515	2.132	0.90	0.6553	29 ± 3	30 ± 3
					1.02	0.6993	31 ± 3	
16EQ28	Distal deposit of Guano lava flow, north of Riobamba city	759,527	9,834,465	2.029	0.17	0.1871	9 ± 5	4 ± 2*
					0.10	0.0955	5 ± 5	
					0.09	0.0965	5 ± 5	
					0.06	0.0598	3 ± 5	
					0.04	0.0409	2 ± 5	
Igualata volcano								
16EQ23	Lava flow, summit	762,559	9,834,762	1.783	4.44	6.9751	374 ± 10	376 ± 10
					3.99	7.0389	378 ± 11	
16EQ14	Distal lava flow, under Mulmul	776,294	9,837,640	1.967	9.78	7.5893	369 ± 6	371 ± 7
					5.62	7.6959	375 ± 9	
16EQ27	Distal SE lava flow	770,383	9,818,984	1.455	12.87	5.4347	358 ± 6	358 ± 6
					11.17	5.4406	358 ± 6	
16EQ24	Lava flow, E flank	765,091	9,834,997	1.320	7.94	4.6095	334 ± 6	337 ± 7
					6.97	4.6994	341 ± 7	
16EQ29	Lava flow, SW flank, Patulù valley	757,733	9,827,827	2.130	2.98	5.2630	237 ± 9	237 ± 9
					2.99	5.2781	237 ± 9	
16EQ30	Pyroclastic flow deposit, SW flank	757,703	9,827,809	3.063	1.04	3.4471	108 ± 10	107 ± 11
					1.02	3.4291	107 ± 11	
Huisla-Mulmul volcanic complex								
16EQ07	Lava flow, W flank	769,568	9,845,822	1.532	10.28	9.9303	621 ± 11	612 ± 10
					15.30	9.7077	607 ± 9	
16EQ04	Lava flow, N flank	771,468	9,849,602	1.838	14.14	11.317	590 ± 9	587 ± 9
					14.15	11.205	584 ± 9	
RIO-107	Lava flow, NW flank	768,948	9,846,937	1.413	6.29	7.9374	538 ± 11	547 ± 11
					6.61	8.2139	557 ± 12	
16EQ05	Lava flow, W flank	769,181	9,845,523	1.328	2.91	7.1965	519 ± 19	526 ± 20
					2.88	7.3924	533 ± 20	
RIO-111	Lava flow, N flank	770,536	9,848,278	2.579	8.97	13.221	491 ± 9	492 ± 9
					9.23	13.278	493 ± 9	
16EQ08	Lava flow, N flank	773,790	9,843,648	1.933	9.42	3.4885	173 ± 3	174 ± 3
					8.14	3.5413	175 ± 3	
16EQ09	Lava flow, N flank	773,525	9,842,805	2.154	4.03	3.6820	164 ± 5	163 ± 5
					4.34	3.6574	163 ± 4	
16EQ10	Lava flow, N flank	773,156	9,842,420	2.073	7.09	3.5358	163 ± 3	163 ± 3
					7.81	3.5441	164 ± 3	
16EQ11	Lava flow, N flank	772,791	9,841,758	1.484	4.10	2.2092	143 ± 4	145 ± 4
					4.15	2.2810	147 ± 4	
Licto and Calpi cones								
16EQ47	Lava flow, Licto cone (Cerro Tulabug)	766,283	9,802,345	1.275	2.24	2.4787	186 ± 9	183 ± 9
					2.15	2.4042	181 ± 9	
17EQ114	Distal lava flow, Calpi, under the DAD of Chimborazo	750,964	9,817,521	1.494	1.58	1.0111	65 ± 4	62 ± 4
					1.50	1.0043	64 ± 4	
					1.30	0.8785	56 ± 4	
16EQ34	Lava flow, Calpi, NW cone	752,666	9,818,239	1.492	0.27	0.2477	16 ± 6	9 ± 3*
					0.20	0.1861	12 ± 6	
					0.13	0.1263	8 ± 6	
					0.11	0.0953	6 ± 6	
					0.07	0.0693	4 ± 6	
16EQ35	Lava flow, Calpi, SW cone	752,117	9,817,907	1.417	0.09	0.1561	11 ± 12	8 ± 5*
					0.09	0.1536	10 ± 12	
					0.07	0.1391	9 ± 13	
					0.04	0.0805	5 ± 13	
					0.02	0.0385	3 ± 12	

Table 2
Major and trace element compositions of whole-rock samples. All major element data were brought down to a total of 100%. Samples marked with an asterisk (*) have not been dated.

	Sagoatoa			Igualata						
	16EQ03	16EQ40	16EQ41*	16EQ14	16EQ22*	16EQ23	16EQ24	16EQ27	16EQ29	16EQ30
wt%										
SiO_2	57.54	63.98	58.13	63.09	53.02	56.32	54.40	61.23	57.81	65.87
TiO_2	0.84	0.90	0.81	0.59	1.09	0.96	1.04	0.62	0.93	0.54
Al_2O_3	15.56	15.32	16.87	16.94	18.32	18.19	16.59	17.41	16.93	16.29
Fe_2O_3	7.49	6.04	7.28	5.17	8.88	7.38	8.99	6.03	7.33	4.36
CaO	6.99	4.59	6.88	5.29	8.16	7.01	7.96	5.81	6.74	4.20
MgO	6.05	2.55	4.66	2.35	5.03	4.00	5.57	2.35	4.18	1.80
MnO	0.11	0.08	0.10	0.09	0.12	0.09	0.12	0.10	0.11	0.06
K_2O	1.25	2.49	1.19	1.77	1.22	1.66	1.32	1.69	1.79	2.38
Na_2O	3.95	3.76	3.89	4.51	3.86	4.10	3.71	4.49	3.89	4.32
P_2O_5	0.23	0.29	0.20	0.19	0.30	0.29	0.30	0.28	0.29	0.18
L.O.I.	0.06	0.80	1.84	0.13	−0.17	1.22	−0.04	0.20	0.59	1.33
ppm										
Sc	18.30	11.88	14.90	9.47	15.80	13.87	16.34	8.52	15.50	6.93
V	187.92	158.16	160.56	106.22	190.51	176.31	210.68	118.90	177.04	90.21
Cr	256.62	49.20	123.16	24.41	124.88	57.29	163.31	21.52	100.32	17.94
Co	29.01	17.22	23.56	12.90	27.64	23.10	29.98	13.73	23.62	11.06
Ni	144.22	47.49	66.01	16.71	58.54	46.54	95.46	17.03	58.89	13.52
Rb	25.89	57.70	28.00	43.91	27.20	43.53	21.54	37.16	45.10	71.36
Sr	536.70	376.50	547.10	616.91	815.67	730.12	926.55	948.97	740.76	534.82
Y	16.34	23.83	13.06	11.80	15.31	15.95	14.68	11.64	15.58	11.17
Zr	129.18	246.62	32.41	128.86	121.67	140.26	118.60	116.87	146.06	145.29
Nb	4.45	9.62	4.90	5.23	7.44	6.40	4.92	4.57	6.64	4.65
Ba	475.42	809.53	574.08	853.96	625.38	719.38	620.08	901.10	793.83	949.89
La	14.06	24.00	14.14	18.77	20.14	20.66	23.52	21.90	20.89	19.33
Ce	31.14	50.40	24.82	37.27	38.82	42.17	47.06	43.74	44.74	41.90
Nd	17.45	27.33	15.55	17.19	24.40	22.99	26.23	21.61	23.34	18.71
Sm	3.62	5.74	2.98	3.40	4.86	4.36	4.75	4.10	4.44	3.66
Eu	1.12	1.36	0.97	0.92	1.37	1.21	1.34	1.19	1.21	0.81
Gd	3.62	5.01	2.77	2.77	4.37	3.92	4.29	3.15	3.84	2.93
Dy	2.86	4.05	2.31	2.16	3.04	2.95	2.72	2.18	2.78	2.06
Er	1.50	2.04	1.02	0.64	1.22	1.41	1.32	0.76	1.52	0.86
Yb	1.45	1.87	0.87	1.04	1.01	1.28	1.07	1.15	1.26	0.87
Th	2.78	6.55	3.16	4.34	3.49	4.31	4.60	5.20	5.06	6.61

	Huisla-Mulmul complex								
	RIO 107	RIO 111	16EQ04	16EQ05	16EQ07	16EQ08	16EQ09	16EQ10	16EQ11
wt%									
SiO_2	54.02	64.66	55.74	55.52	56.92	60.35	60.72	61.08	52.83
TiO_2	0.98	0.58	0.93	0.94	0.97	0.77	0.74	0.77	0.97
Al_2O_3	18.85	16.58	18.39	17.48	17.52	17.81	17.76	17.37	18.47
Fe_2O_3	8.38	4.69	7.98	8.27	7.92	6.22	6.40	6.31	9.05
CaO	7.24	4.57	6.80	7.44	6.97	5.72	5.43	5.59	8.20
MgO	4.59	2.10	3.73	4.78	3.89	2.49	2.24	2.47	5.23
MnO	0.13	0.08	0.12	0.13	0.11	0.10	0.10	0.11	0.15
K_2O	1.41	2.64	1.69	1.38	1.51	2.12	2.09	2.04	1.37
Na_2O	4.08	3.94	4.29	3.81	3.92	4.21	4.26	4.03	3.52
P_2O_5	0.32	0.17	0.33	0.25	0.27	0.23	0.25	0.22	0.22
L.O.I.	0.56	1.20	0.06	0.31	0.51	0.96	0.01	0.06	−0.18
ppm									
Sc	16.46	9.02	12.95	18.91	16.90	11.74	9.48	12.45	25.51
V	209.32	89.23	186.12	178.00	196.57	150.78	123.52	140.61	227.85
Cr	90.20	36.43	69.96	76.48	47.81	5.48	7.10	9.55	42.69
Co	26.39	11.43	26.38	27.27	23.51	15.43	15.14	15.03	28.54
Ni	52.98	19.00	49.02	49.75	30.18	5.36	3.99	7.69	24.18
Rb	52.98	69.84	36.10	27.23	32.42	57.85	63.30	62.37	35.60
Sr	1007.07	541.17	976.12	733.36	726.42	662.15	611.23	542.43	632.07
Y	15.58	13.02	15.36	15.08	16.16	15.10	17.52	19.04	24.73
Zr	113.89	168.84	121.00	110.44	112.94	132.16	151.88	145.22	112.77
Nb	6.79	7.92	6.38	5.22	5.97	5.90	7.02	5.99	5.16
Ba	874.25	1068.14	913.17	705.75	722.53	927.85	870.18	845.11	675.19
La	20.50	22.76	22.42	15.79	18.98	18.85	20.99	20.10	17.95
Ce	37.59	41.38	43.39	34.24	34.30	39.58	42.29	40.38	35.72
Nd	22.17	18.26	23.04	18.44	20.02	18.40	20.88	20.54	20.60
Sm	4.30	3.31	4.69	4.60	3.87	3.70	4.70	3.75	4.57
Eu	1.27	0.93	1.36	1.19	1.15	1.01	1.16	1.12	1.20
Gd	3.78	2.70	3.82	3.55	3.63	3.40	4.17	3.87	4.52

(*continued on next page*)

Table 2 (*continued*)

	Huisla-Mulmul complex								
	RIO 107	RIO 111	16EQ04	16EQ05	16EQ07	16EQ08	16EQ09	16EQ10	16EQ11
Dy	2.81	2.22	2.82	2.62	2.78	2.55	3.06	3.12	4.25
Er	1.23	1.05	1.59	1.16	1.35	1.31	1.21	1.75	2.32
Yb	1.25	1.12	1.21	1.25	1.25	1.35	1.52	1.63	2.29
Th	3.69	8.07	4.10	2.92	3.04	5.58	6.90	6.49	4.27

	Carihuairazo		Guano lava flow		Licto cone	Calpi cones		
	CAR-14	RIO-18	16EQ28	16EQ43	16EQ47	16EQ34	16EQ35	17EQ114
wt%								
SiO_2	59.62	54.71	61.73	61.96	53.08	61.07	54.65	60.90
TiO_2	0.76	0.76	0.72	0.71	0.97	0.73	0.92	0.73
Al_2O_3	17.52	16.06	16.39	16.35	15.99	16.02	15.98	16.24
Fe_2O_3	6.44	8.18	6.00	5.98	8.84	6.15	7.67	6.24
CaO	6.11	9.08	5.66	5.44	8.16	5.74	7.86	5.85
MgO	3.51	5.77	3.21	3.26	7.84	4.23	6.96	4.10
MnO	0.10	0.12	0.09	0.08	0.13	0.08	0.12	0.09
K_2O	1.31	1.44	1.79	1.84	1.24	1.58	1.45	1.52
Na_2O	4.41	3.61	4.22	4.17	3.50	4.21	4.03	4.14
P_2O_5	0.22	0.26	0.20	0.20	0.25	0.19	0.36	0.20
L.O.I.	0.12	0.21	0.34	0.16	0.26	0.70	0.12	0.72
ppm								
Sc	13.17	26.00	13.11	12.53	20.85	12.79	18.49	12.39
V	146.54	220.00	143.99	139.08	205.34	145.83	197.08	146.83
Cr	53.58	156.00	56.76	64.73	362.66	193.05	283.17	164.81
Co	20.72	28.00	18.07	17.53	35.86	20.79	31.35	23.44
Ni	46.72	41.00	40.57	48.73	172.54	75.66	136.86	74.25
Rb	17.03	20.00	41.88	45.77	19.36	38.16	27.19	34.35
Sr	692.38	1145.00	578.33	557.92	700.83	562.84	930.73	642.81
Y	11.41	16.90	13.54	13.49	14.07	9.84	13.51	12.12
Zr	104.51	102.00	150.12	149.59	98.96	106.90	109.85	110.43
Nb	4.56	4.10	5.16	6.02	5.34	4.03	8.84	5.44
Ba	610.68	945.00	745.61	840.39	595.85	645.29	776.47	696.31
La	13.06	32.00	16.68	17.38	14.68	13.53	20.97	14.31
Ce	26.87	60.00	33.77	36.73	31.43	28.29	43.17	29.28
Nd	15.52	30.00	18.42	18.74	17.55	15.16	22.43	15.69
Sm	3.46	6.05	3.64	3.43	3.74	2.88	4.55	3.42
Eu	1.02	1.48	0.98	1.08	1.13	0.98	1.22	0.98
Gd	2.87	4.30	3.32	3.32	3.50	2.54	3.67	2.99
Dy	2.06	3.10	2.33	2.34	2.65	1.81	2.44	1.70
Er	0.32	1.70	1.23	1.26	1.50	0.41	1.01	1.10
Yb	0.97	1.64	1.16	1.04	1.06	0.78	1.03	0.77
Th	2.43	7.60	4.17	4.54	2.21	3.30	4.09	3.34

magmas. The content of incompatible elements is similar to our samples, except for Y and the heavy REE (HREE; Dy, Er, Yb), which are enriched in samples of Mulmul and Sagoatoa volcanoes (red and pink lines respectively; Fig. 3b and c). Finally, the content of major, trace and incompatible elements is similar for both ***Guano lava flows***.

Crustal processes such as fractional crystallization govern the composition of lava flows, yielding a negative correlation between compatible elements (e.g., MgO, Fe_2O_3, CaO, Cr, Ni; Fig. 4a and b) and SiO_2, due to the crystallization of olivine, pyroxene, Fe-Ti oxide and plagioclase phenocrysts in the magma chamber, and a positive correlation for Na_2O (Fig. 4c) and for incompatible elements (e.g., Rb and Ba; Fig. 4d). These trends are in agreement with previous analyses carried out on other volcanoes from the southern part of the arc (grey dots in Fig. 4), including lavas from Tungurahua, Chimborazo, Huisla, and Sangay. However, there is no single and unequivocal interpretation about the origin of the temporal variation of the geochemistry, which may be related to changes in the deep mantle source or crustal processes. Our data, despite age differences, reflect the same macro-process related to the subduction context, and do not result from local, superficial or minor phenomena. For that reason, we prefer not to use these major and trace element analyses for interpretative purposes about volcanism-geodynamics relationships.

5. Discussion

5.1. Comparison with previously published data

Our new ages (Table 1) are in the range of those previously reported at Carihuairazo, Chimborazo and Tungurahua volcanoes (Barba et al., 2008; Samaniego et al., 2012; Le Pennec et al., 2013; Bablon et al., 2018a). However, both ages from ***Sagoatoa*** volcano are younger than published K-Ar whole-rock and plagioclase ages (1.73 ± 0.35 and 1.40 ± 0.29 Ma respectively; Lavenu et al., 1992), obtained for the same lava flow as 16EQ03 (799 ± 12 ka), and for a lava flow located on the eastern flank of the volcano, respectively. This large difference of about 1 Ma can be explained by the presence of inherited radiogenic argon in the phenocrysts, which are necessarily included in the whole-rock analysis. Indeed, if they were incorporated late in the magma chamber, they did not have time to be reset before the eruption, hence producing a bias towards older values for the whole-rock ages. Whole-rock samples may also contain concealed weathered areas, where the potassium may have been leached, and, hence, this will also induce too old ages.

The age obtained for Tzunantza dome (512 ± 9 ka), north of ***Carihuairazo*** volcano, is significantly older than lava flows of its

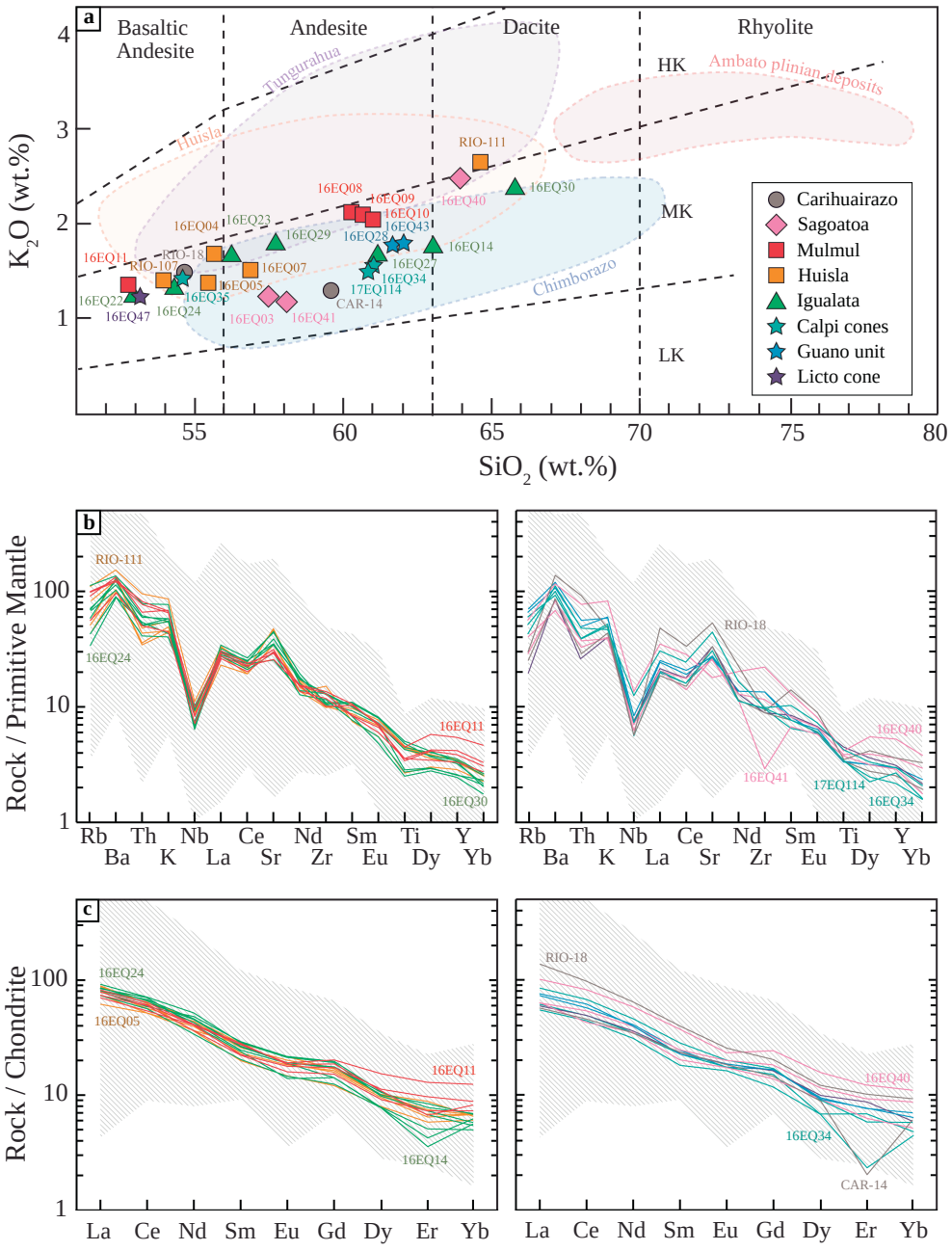

Fig. 3. a) K_2O vs. SiO_2 diagram (Peccerillo and Taylor, 1976) for samples analyzed in this study. Composition fields of previous data are reported in the background, for Huisla (orange; Bustillos, 2008), Tungurahua (purple; Schiano et al., 2010; Samaniego et al., 2011; Le Pennec et al., 2013; Bablon et al., 2018a), Chimborazo (blue; Samaniego et al., 2012), and Ambato plinian fall deposits (red; Ordóñez, 2012). HK: high-K calc-alkaline series, MK: medium-K calc-alkaline series, LK: low-K calc-alkaline series. b) Trace elements normalized to primitive mantle spider diagram (Sun and McDonough, 1989). Spectra for Huisla (orange), Mulmul (red) and Igualata (green) volcanoes are shown in the left diagram, and those of Carihuairazo (brown), Sagoatoa (pink), Guano (blue), Calpi (turquoise) and Licto (purple) in the right diagram. Hatched grey domain represents whole-rock data of the entire Ecuadorian arc (GEOROC database; http://georoc.mpch-mainz.gwdg.de/georoc/). c) Rare Earth Elements normalized to chondrites diagram (Sun and McDonough, 1989). Same legend as in Fig. 3b. (For interpretation of the references to colour in this figure legend, the reader is referred to the web version of this article.)

southern flank, dated at ~225 ka (Samaniego et al., 2012). We thus propose that this new age may correspond to an older, pre-Carihuairazo volcanic activity. Moreover, the lava sample of ***Puñalica*** edifice, dated at 18 ± 3 ka, confirms that it was constructed at the end of the LGM, before the emplacement of the younger moraines during the Younger Dryas (10–12 ka; Clapperton, 1990).

Further to the south, the Riobamba basin is filled by 10–12 km^3 of debris avalanche deposits from the huge sector collapse of Chimborazo volcano (Bernard et al., 2008; Samaniego et al., 2012). The avalanche deposit related to this event is locally covered by the distal ***Guano lava flows*** unit, the LGM moraines (18–25 ka), and the Río Blanco ash flow sequence (42–43 ka; Samaniego et al., 2012). The age of 30 ± 3 ka, obtained here for a proximal lava flow from the Guano unit, yields a maximum age for the LGM (Clapperton, 1990). Moreover, it implies that the sector collapse occurred before 30 ka, which is roughly in agreement with the stratigraphic data and the ages of Samaniego et al. (2012). However, the age obtained for the distal Guano lava flow (4 ± 2 ka), whose levees are well preserved (Fig. 5a), is significantly younger than the previously published $^{40}Ar/^{39}Ar$ groundmass age of 60 ± 11 ka (sample RIO-5; Samaniego et al., 2012). Unfortunately, this age is not supported by any $^{40}Ar/^{39}Ar$ age spectra, nor inverse isochron. Furthermore, it was the only age from that study that was obtained using stepwise laser heating, hence without temperature control (M. Fornari, pers. com.). The lack of detail information prevents us from explaining such large differences, but we note that the groundmass fraction used for $^{40}Ar/^{39}Ar$ dating was selected by hand, without using heavy liquids to obtain a narrow density range (2.53–2.60), as was the case here for K-Ar dating. Similarly, undetected ^{39}Ar recoil, occurring during irradiation, could also have significantly biased the $^{40}Ar/^{39}Ar$ results. The elevation profile of the valley across the distal Guano lava flow (Fig. 5c) shows that a ~120 m-thick sequence of the Chimborazo avalanche deposits, which also crop out on the southern flank of Igualata volcano (Bernard et al., 2008), was eroded by the San Andrés river before the emission of this lava flow. The fact that the base of the flow is at the same elevation as the present day bottom of the valley (Fig. 5c) strongly suggests that the river had no

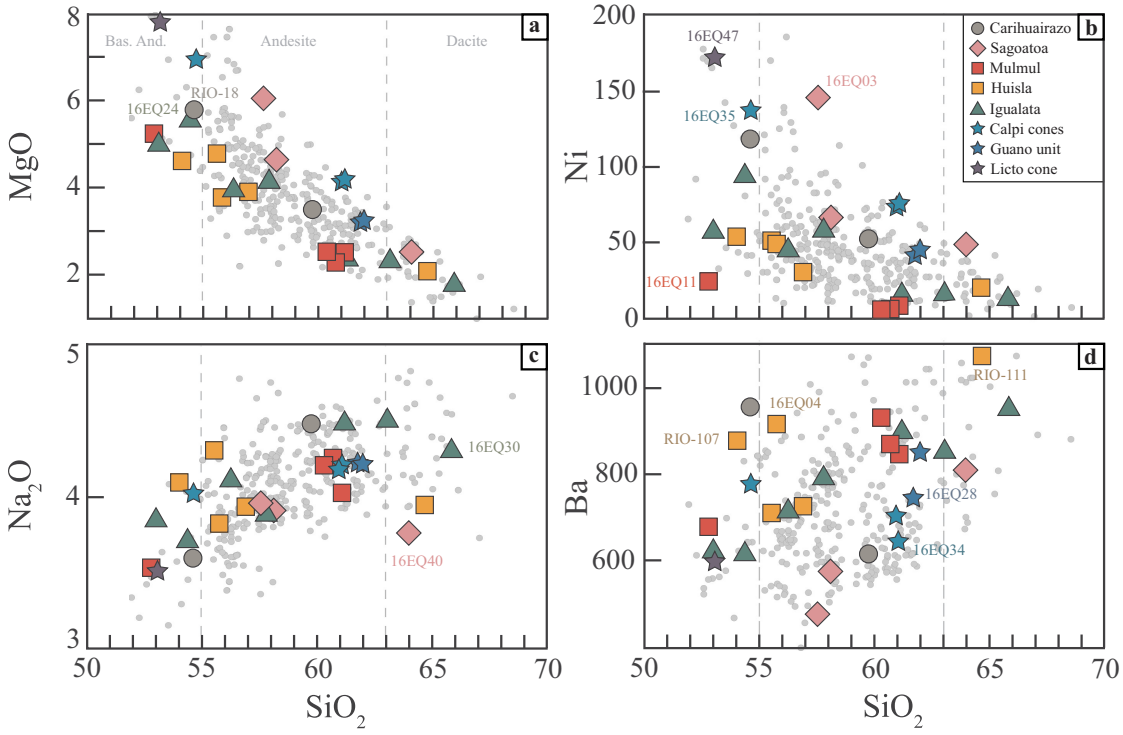

Fig. 4. Diagrams of some major and trace elements, plotted against silica. a–c) Harker diagrams for MgO and Na_2O, respectively (in wt%). Bas. And.: basaltic andesite. b–d) Variation diagrams for Ni and Ba, respectively (in ppm). Symbols are the same as in Fig. 3a. Small grey dots are previously published data for volcanoes located in the southern part of the Ecuadorian arc (Barberi et al., 1988; Barragán et al., 1998; Bryantet al., 2006; Hoffer et al., 2008; Schiano et al., 2010; Samaniego et al., 2011; Hidalgo et al., 2012; Ancellin et al., 2017; Bablon et al., 2018a).

time to further incise the valley, and argues in favor of the very young age of 4 ± 2 ka obtained from our measurements (16EQ28; Table 1). Finally, this age implies that Guano lava flows were emitted as two different units. An older proximal unit was erupted after the sector collapse of Chimborazo and before the LGM period, whereas a younger unit includes the distal lava flow. This suggests that a pulse of lava emission occurred during the Holocene, probably associated with the explosive activity reported by Barba et al. (2008).

It was previously described that the Chimborazo collapse deposits cover scoria fallouts from ***Calpi cones*** located southwest of the Riobamba basin (Bernard et al., 2008). New field observations indicate that a distal lava flow can be also related to the activity of Calpi cones. The distal lava flow from Calpi cones is unambiguously covered by the debris avalanche and tephra fallout deposits from Chimborazo volcano, while Calpi proximal lavas do not seem covered by any volcanic product. Consequently, Calpi cones could have been constructed in at least two stages. The remnants of the oldest stage, represented by the distal lava flow that lies under the collapse deposits, were emitted at 62 ± 4 ka (17EQ114), while we have dated the youngest stage at 9 ± 3 and 8 ± 5 ka (16EQ34 and 16EQ35; Table 1), which is responsible of the formation of the cones and proximal lava flows. Directly overlying the lava flow of the oldest construction stage, the debris avalanche deposits emplaced during the Chimborazo major sector collapse have therefore a well constrain maximum age of 62 ± 4 ka. This new age confirms the previous hypothesis that the sector collapse event occurred ~65–60 ka, based on stratigraphy and $^{40}Ar/^{36}Ar$ ages of Chimborazo lava flows (Samaniego et al., 2012).

Although no lava flow from ***Huisla*** volcano was previously dated, three plinian fallout deposits, exposed in the Ambato basin (Fig. 2a), have been attributed to the late activity of this volcano (Ordóñez, 2012). They contain grey and white pumice clasts, crystals of plagioclase, amphibole, pyroxene and biotite, as well as some metamorphic clasts with a petrography close to the basement of the Eastern Cordillera, and andesite clasts similar to lava flows of the Huisla-Mulmul complex (Ordóñez, 2012) and incorporated during magma ascent. According to uncalibrated ^{14}C age determinations, the two younger tephra fallout deposits were erupted during the last 40 ka, while the first plinian eruption is older (Ordóñez, 2012). However, our ages indicate that Huisla volcano was constructed between 612 ± 10 ka and 492 ± 9 ka, and collapsed before the onset of ***Mulmul*** construction, dated here at ~180 ka (Fig. 5b; Table 1). As there is no evidence of activity for Huisla volcano after its sector collapse, the proposed age of the tephra fallout deposits, in particular for the two younger plinian eruptions, is therefore much too young to be associated with Huisla volcano. On the other hand, Mulmul volcano is younger than 180 ka, with major element compositions of its lavas similar to those of Huisla (Fig. 3a; Fig. 4). Therefore, we suggest that plinian fall deposits of the Ambato basin may originate from a late activity of Mulmul volcano. This hypothesis remains consistent with the isopach maps (Ordóñez, 2012), although no proximal tephra fallout deposit seems to crop out in the vicinity of Mulmul. Moreover, based on stratigraphy, Bustillos (2008) and Espín (2014) showed that Huisla sector collapse is younger than the Chalupas ignimbrite, dated at ~215 ka (Beate et al., 2006; Bablon et al., 2018b). Since this destabilization occurred before the construction of Mulmul volcano, which is partly constructed inside the amphitheater, we therefore propose that the sector collapse of Huisla volcano occurred between 215 and 180 ka.

5.2. *Edifice history of the southern arc volcanism*

Based on our new data and previous studies of Chimborazo, Tungurahua and Sangay volcanoes (Monzier et al., 1999b; Samaniego et al., 2012; Bablon et al., 2018a), a reconstruction of the eruptive history of the *E*-W section from the southern Ecuadorian arc can be proposed as follows.

The development of the southern part of the arc began with the construction of the andesitic ***Huisla*** volcano in the Interandean Valley, around 600 ka. Before, the southernmost edifice of the Middle

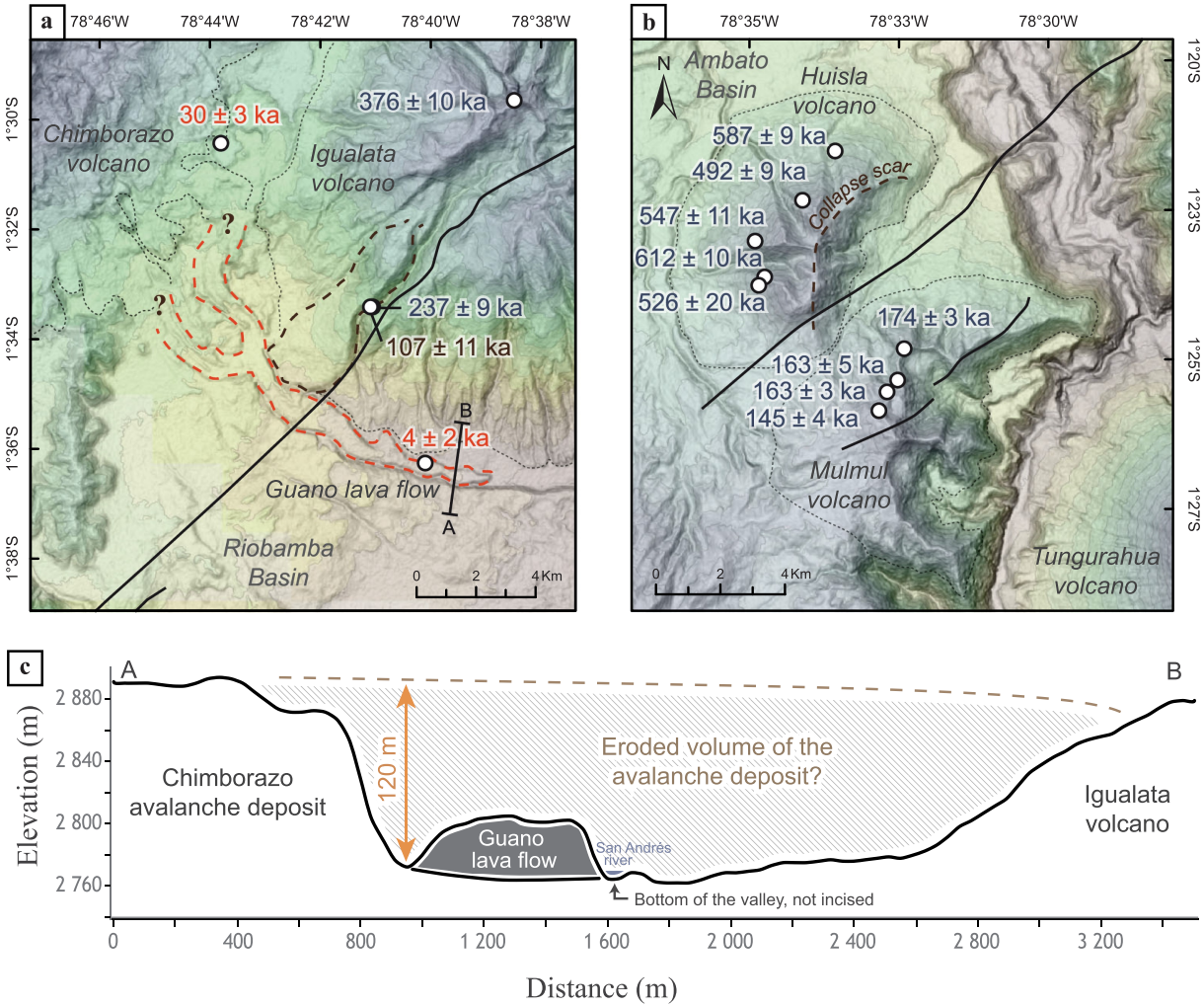

Fig. 5. Four meters resolution DEM (Sigtierras; http://www.sigtierras.gob.ec/) of the southwestern flank of a) Igualata volcano and the Guano lava flow, and b) Huisla and Mulmul volcanoes. K-Ar ages obtained here and location of the Pallatanga fault (black line) are also shown. Outlines of volcanoes are represented by dashed lines. c) Current elevation profile of the San Andres valley and Guano lava flow (vertical exaggeration of 5), between the northern edge of the Chimborazo avalanche deposit (A) and the southern flank of Igualata volcano (B). The profile location is indicated in Fig. 4a.

Pleistocene arc was probably ***Sagoatoa*** volcano, which was constructed before 800 ka (Fig. 6a and b). Huisla volcano activity ended ~500 ka ago, when andesitic domes were emplaced at the current location of ***Carihuairazo*** volcano, in the Western Cordillera. This activity was probably followed by the onset of ***Igualata*** and ***Sangay*** construction, older than 400 ka (Monzier et al., 1999b). At 300 ka, the end of construction of the main edifice of Igualata volcano (Fig. 6c) was coeval with the onset of ***Tungurahua*** activity, in the Eastern Cordillera (Fig. 6d; Bablon et al., 2018a). Then, the volcanic activity seems to increase between 300 and 100 ka (Fig. 6d and e), with the construction of Carihuairazo (Samaniego et al., 2012), and Tungurahua (Bablon et al., 2018a) volcanoes, then those of ***Licto cone***, ***Mulmul*** volcano and ***Puyo cones*** in the back-arc (Hoffer et al., 2008), as well as the onset of ***Chimborazo*** activity ~120 ka (Samaniego et al., 2012). The construction of Mulmul volcano followed the Huisla sector collapse (Fig. 6c) and the large ignimbrite eruption of ***Chalupas*** caldera that occurred at ~215 ka, 75 km to the north (Beate et al., 2006; Bablon et al., 2018b). The construction stages of ***Altar*** volcano, located south of Tungurahua volcano (Fig. 1b), are poorly documented, but it started before ~35 ka since its debris avalanche deposit related to its western flank collapse crops out under the Tungurahua DAD (Bustillos, 2008) dated at that age (Le Pennec et al., 2013). At least seven major sector collapses occurred within the last 100 ka. They are evidenced by the debris avalanche deposits from Chimborazo in the Riobamba basin (Clapperton, 1990; Bernard et al., 2008; Samaniego et al., 2012), from Carihuairazo in the Ambato basin, and from Altar and Tungurahua in Chambo and Pastaza valleys (Hall et al., 1999; Bernard et al., 2008; Bustillos, 2008; Bablon et al., 2018a; Fig. 2). In addition, Mulmul volcano reactivated and produced at least three plinian eruptions, whose deposits are found in the Ambato basin, interbedded with the avalanche deposits of Carihuairazo volcano (Fig. 6f; Ordóñez, 2012). Finally, the volcanic activity of Tungurahua continued during the Holocene, as well as the construction of ***Puñalica***, Sangay volcano (Monzier et al., 1999b), the youngest construction stage of ***Calpi cones*** (Fig. 6f), and the emission of the ~15 km-long distal ***Guano lava flow*** from Chimborazo volcano.

5.3. Relationship between volcanism and the deep geometry of the slab

Overall, the development of volcanoes from the southern Ecuadorian arc seems to have migrated southward. Such migration can also be inferred at larger scale. Indeed, the onset of volcanism in the northern part of the Ecuadorian arc is older than for volcanoes from the southern part (Fig. 7). Although many edifices remain to be studied in detail, such as Altar and Sangay volcanoes, we point out that northern edifices began their activity earlier or close to 1 Ma (Cayambe, Pichincha, Chacana, Pan de Azúcar and Atacazo, for instance; Samaniego

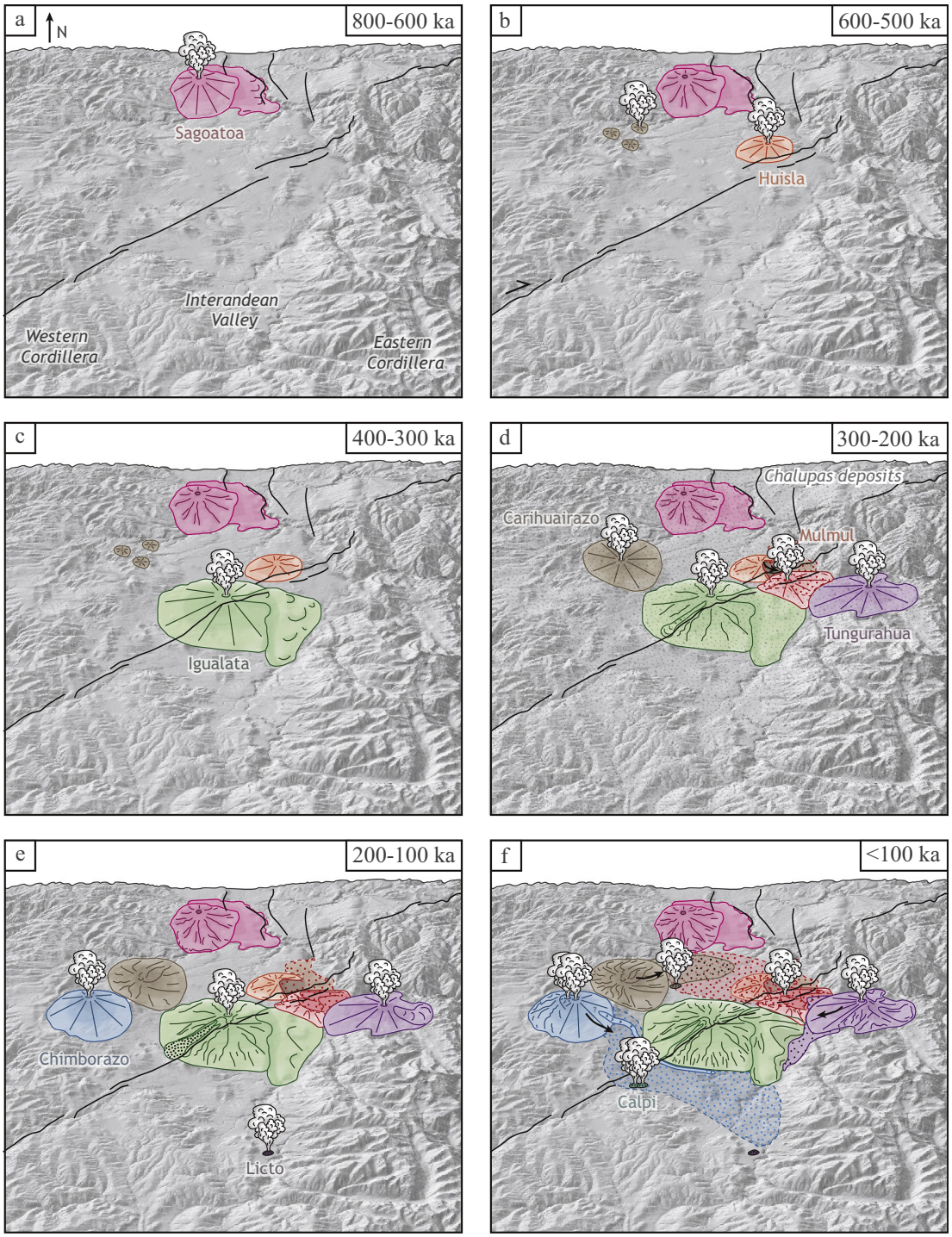

Fig. 6. Synthesis cartoons of the volcanic history of the southern Ecuadorian arc. Construction of a) Sagoatoa volcano (pink) before 800 ka, b) Huisla volcano (orange) and Tzunantza dome (brown), between 600 and 500 ka, c) Igualata volcano (green) between 400 and 300 ka, d) Tungurahua (purple), Mulmul (red) and Carihuairazo (brown) volcanoes, between 300 and 200 ka. During the latter interval, the southeastern flank of Huila volcano collapsed, and Chalupas volcano (Beate et al., 2006; Bablon et al., 2018b) produced the Chalupas ignimbrite deposited throughout the southern Inter-Andean valley at about 215 ka, e) Construction of Licto cone (dark purple) and Chimborazo volcano (blue), together with deposit of pyroclastic flows in the southwestern flank of Igualata volcano (black dots) took place between 200 and 100 ka. f) Sector collapse of Chimborazo, Carihuairazo and Tungurahua occurred in the last 100 ka, during the construction of Puñalica (brown) and Calpi (turquoise) cones, the deposits of plinian eruptions of Mulmul in the Ambato basin (red points), and the eruption of Chimborazo volcano, which produced the distal Guano lava flow (blue). Note that the landscape morphology before the construction of the volcanoes, as well as the erosion of their flanks, are speculative. Altar and Pilisurco volcanoes (Fig. 1b), whose period of construction is too poorly constrained, are not shown. Black lines indicate the location of the Pallatanga fault (Baize et al., 2016).(For interpretation of the references to colour in this figure legend, the reader is referred to the web version of this article.)

et al., 2005; Opdyke et al., 2006; Hidalgo et al., 2008; Hoffer, 2008; Robin et al., 2010), while volcanic activity in the southern arc started later and is younger than 0.6 Ma.

In general, the volcanic front corresponds to the line formed by the volcanoes closest to the subduction zone and generally parallel to the trench axis. These edifices are typically located about 105–110 km

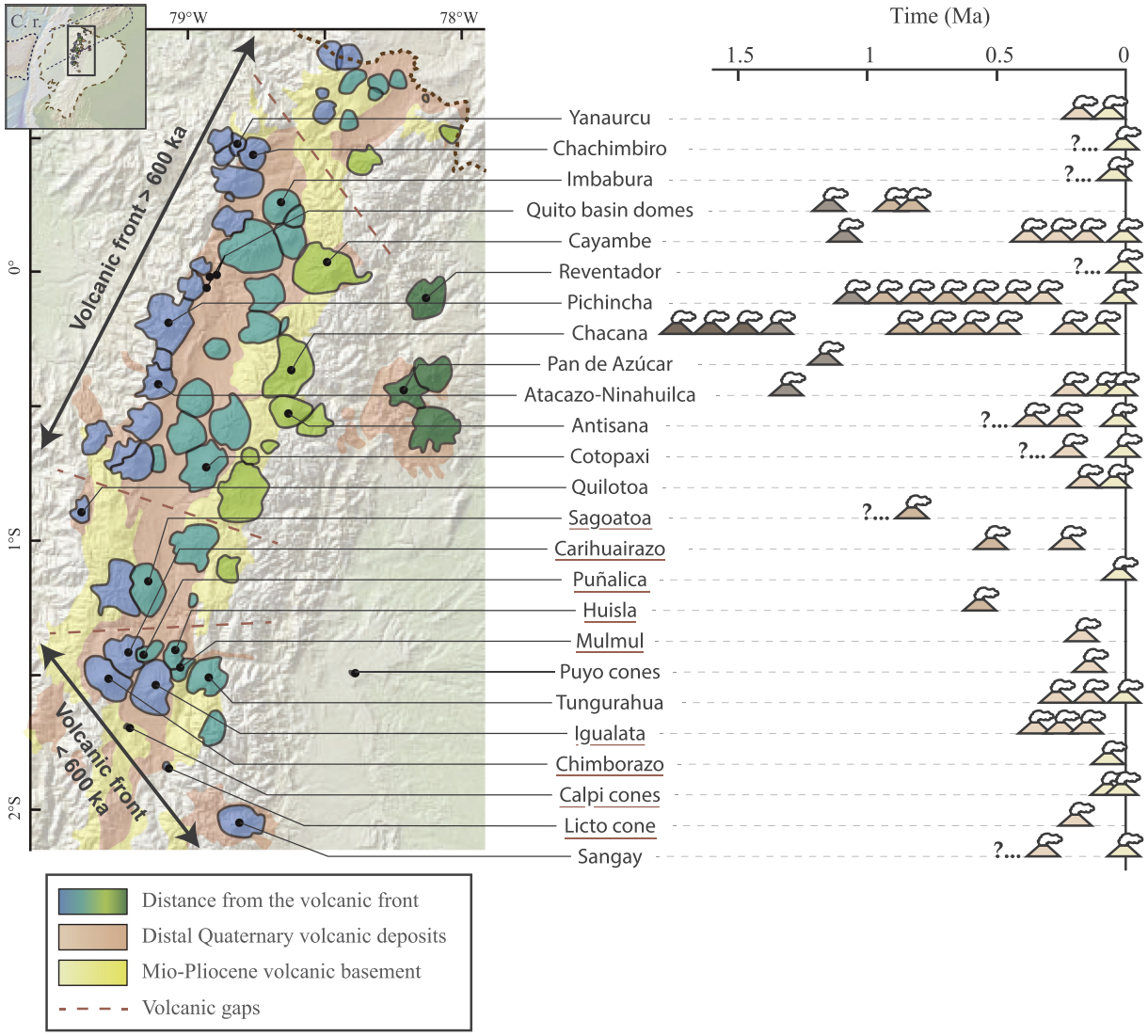

Fig. 7. Chronological synthesis for activity periods of Ecuadorian volcanoes. It shows that the onset of activities seems to be younger in the southern termination of the arc than to the north. Note that we selected only published ages measured using calibrated radiocarbon, $^{40}Ar/^{39}Ar$, and groundmass K-Ar techniques (Samaniego et al., 1998; Hall et al., 1999; Monzier et al., 1999b; Samaniego et al., 2005; Hidalgo, 2006; Opdyke et al., 2006; Barba et al., 2008; Hall and Mothes, 2008; Hidalgo et al., 2008; Hoffer, 2008; Robin et al., 2010; Le Pennec et al., 2011; Samaniego et al., 2012; Le Pennec et al., 2013; Alvarado et al., 2014; Bernard et al., 2014; Béguelin et al., 2015; Hall et al., 2017; Bablon et al., 2018a). Brown dotted lines represent borders of Ecuador. Border and inferred prolongation of the Carnegie ridge (C.r.; Gutscher et al., 1999) are represented by blue dotted lines. Volcanic edifices with new ages obtained in this study are underlined in red. (For interpretation of the references to colour in this figure legend, the reader is referred to the web version of this article.)

above the dipping plate (e.g., Tatsumi, 1986; England et al., 2004; Syracuse and Abers, 2006), where the temperature and pressure conditions allow melting of the mantle wedge and magma genesis. In Ecuador, the depth of the slab below the volcanic front varies between 85 and 100 km for the northern part of the arc, and between 100 and 130 km for southern termination (Fig. 8). Moreover, the distribution of volcanoes along the Ecuadorian arc is not uniform. At least four volcanic clusters stand out, separated by along-arc segments without Quaternary volcanic activity (Fig. 7). For these segments, the spacing between volcanic centers is greater than the volcano-spacing average of ~25 km (Fig. 7). To the north, the Colombian arc consists of a single alignment of volcanoes (Hall and Wood, 1985), which extends into northern Ecuador, forming a first volcanic group of rather small-size edifices, less than 10 km wide (Fig. 7). Further south, separated from the first cluster by a 20–25 km interval without Quaternary volcanic activity, the second group extends from Chachimbiro to Iliniza volcanoes (Fig. 7) and includes the greatest number of volcanoes and back-arc volcanism. The width of the arc increases significantly between 0.5°N and 1°S and reaches 140 km wide, in front of the subducting Carnegie ridge (Fig. 1a). Southward, where the volcanic activity is younger, the arc becomes narrower again. The third group of volcanoes is mainly represented by Pilisurco-Sagoatoa complex, Chinibano and Quilotoa volcanoes (Fig. 1b and 7). They are separated from the previous group by about 35 km, where only Quilotoa volcano, the westernmost edifice, is constructed. Finally, south of a 10 km wide interval without Quaternary edifices, the fourth group consists of the southern termination of the Ecuadorian arc, and ends with a single edifice, Sangay volcano. The northeastern Japan arc presents similar volcanic clusters, interpreted as a result of thermal anomalies within the mantle wedge, which increase melting rate and magma production (Tamura et al., 2002). Moreover, the geographic orientation of the Ecuadorian Quaternary arc changes significantly from the northern to the younger southern part, although it seems to have been rather straight during the Pliocene (yellow areas west of Chimborazo volcano; Fig. 7). More specifically, the line formed by the volcanic front in Colombia has a NE trending orientation, which changes to a NNE trend in northern and

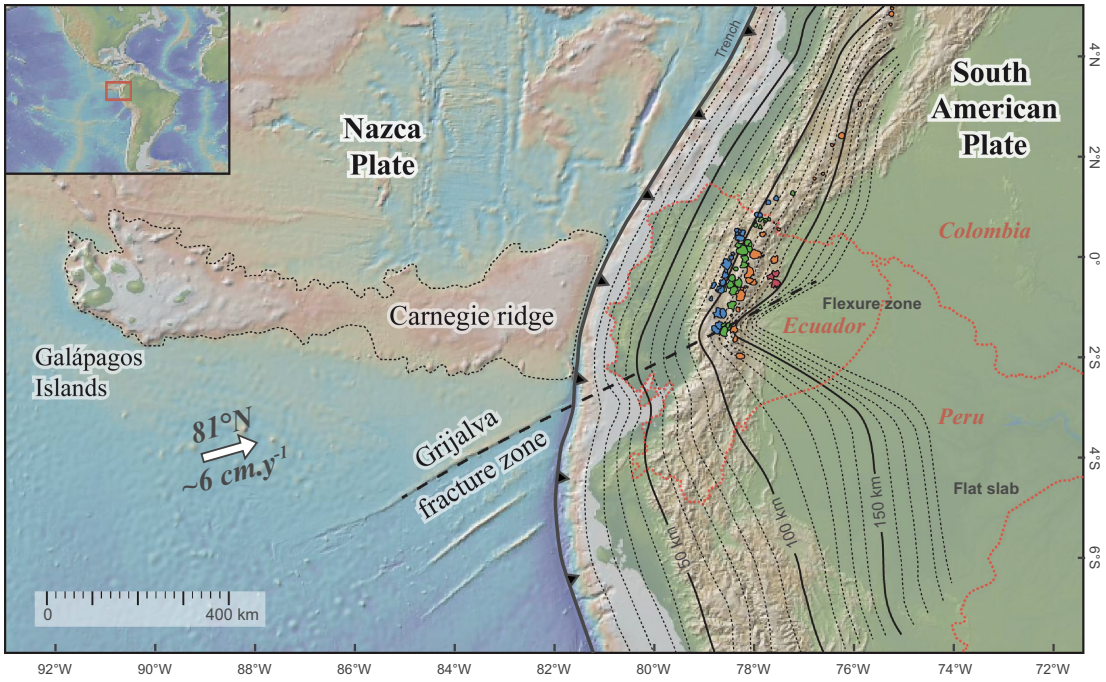

Fig. 8. Geodynamic setting of Ecuador, showing the relationship between the Carnegie Ridge, originating from the Galápagos hot spot activity, the Grijalva fracture zone, the geometry of the slab at depth (modified from Hayes et al., 2012; Yepes et al., 2016) and the Quaternary arc (modified from Hall and Wood, 1985; Hall et al., 2008). The white arrow indicates the direction of the Nazca plate motion relative to South America (DeMets et al., 2010; Nocquet et al., 2014).

central Ecuador, then to a NW trend in the southern part of the arc, south of 1°S. A recent seismic study focused on the geometry of the slab below Ecuador has shown that the subduction of the Grijalva fracture zone between Farallón and Nazca plates (Fig. 1a), as well as the change of convergence obliquity resulting from the convex shape of the continental margin, produces a flexure of the slab at depth (Yepes et al., 2016; Fig. 8). We observe that the young volcanoes from the southern termination of the arc investigated here are located just above this flexure. By contrast, volcanoes with an older activity are located above an area where the dip of the slab is shallower (Yepes et al., 2016; Fig. 8), whereas only two Quaternary edifices (Sangay and Altar volcanoes) are present south of the Grijalva fracture zone prolongation. We infer that the regional volcanism and the development of the arc are related to the slab geometry at depth. Consequently, the curvature of the volcanic front could have been initiated by the change in the slope of the slab induced by the flexure area, while the recent southward migration of volcanic activity highlighted here may have been partly triggered by a displacement of both the flexure and the Grijalva fracture zone at depth below the arc in the last 600 ka. Indeed, the fast and oblique convergence of the Nazca plate may induce a translation of the Grijalva fracture zone, and then, a displacement of the slab flexure southward through time. The resulting changes of pressure and temperature conditions may favor mantle partial melting, and hence magma genesis. Such relationships between the slab geometry and the volcanism migration have been previously described in the Central Andes (e.g., Ramos and Folguera, 2005, 2009). Assuming that the average velocity and motion direction of the Nazca plate during the last million years is similar to the current GPS data (~6 cm·a^{-1} and ~N81°E relative to South America; Trenkamp et al., 2002; Kendrick et al., 2003; Bird, 2003; DeMets et al., 2010; Nocquet et al., 2014), that the angle between the Grijalva fracture zone and the motion direction of the Nazca plate $\theta_{Grij-Nazca}$ is 10 ± 1°, that the angle between the Grijalva fracture zone and the margin $\theta_{Grij-margin}$ is 45 ± 5° (Fig. 8), and using the same approach as used by Hampel (2002) to estimate the displacement of the Nazca ridge in Peru, we propose that the southward translation of the Grijalva fracture zone along the trench occurred at $V = \frac{V_{Nazca} \cdot \sin(\theta_{Grij-Nazca})}{\sin(\theta_{Grij-margin})} = 15 \pm 1$ km·Ma^{-1}. Such value is in agreement with the paleogeographic reconstructions of the Nazca plate based on marine magnetic anomalies and the inferred past location of the Grijalva fracture zone (Hey, 1977; Meschede and Barckhausen, 2001; Collot et al., 2009). However, this velocity seems too low to account alone for the southward volcanism migration since 600 ka, and a slab deformation without a significant displacement of the Grijalva fracture zone may have occurred to explain the distribution of volcanoes along the southern Ecuadorian arc.

5.4. Relationship between volcanism and crustal fault activity

The intense volcanic activity since ~500 ka and the numerous sector collapse events that seem to occur in the last 100 ka in the southern termination of the arc may also be interpreted in light of the tectonic activity occurring along the Chingual-Cosanga-Pallatanga-Puná (CCPP; Alvarado et al., 2016; Fig. 1a) fault system, and especially along the Pallatanga fault segment. Several edifices, such as Calpi cones, Igualata, Huisla, and Mulmul volcanoes, line up with the fault (Figs. 2b,6). Their location and morphology suggest a close relationship between the tectonic activity of the Pallatanga fault and the location and evolution of volcanoes within the Interandean Valley. The volcanic edifice construction that appears to be most affected by the interaction with the tectonic activity is ***Igualata*** volcano. The construction of its main structure occurred approximately between 380 and 350 ka (Table 1). Then, after an apparent period of quiescence of ~100 ka, it experienced at least two periods of activity, at 237 ± 9 ka with the andesitic lava flow, and at 107 ± 11 ka with the three dacitic pyroclastic flows unit. Both units were emitted along the Pallatanga fault (Baize et al., 2016). Moreover, their emplacement within the Patalú valley (Fig. 2c) incised by the recurring seismic activity of the Pallatanga segment strongly suggests that the fault had already an impact on the morphology at ~250 ka, and therefore that it was already active at that time. In the southern foothill of Igualata volcano, the distal ***Guano lava flow*** is sheared by the Pallatanga fault (Fig. 4a). Taking into account its age of 4 ± 2 ka (Table 1) and a lateral offset of at least 20 m

(Baize et al., 2016), a displacement velocity of 3.3 to 10 mm·a^{-1} can be calculated. This result is in agreement with the Holocene slip rate obtained for the Pallatanga fault (Winter et al., 1993) and GPS data for the bulk CCPP fault velocity (Nocquet et al., 2014). Further south, ***Calpi cones*** are quite isolated from other volcanoes and sit along the fault system, southwest of the Riobamba basin (Fig. 6). Characterized by a relatively primitive composition (Monzier et al., 1999a; Ancellin et al., 2017; Fig. 3a), their eruption could have been favored by fracture openings along the fault possibly following large earthquakes. Similarly, ***Huisla*** and ***Mulmul*** volcanoes are constructed at the intersection between the northeastern known tip of the Pallatanga fault and a N-S suture zone located along the Eastern Cordillera (Alvarado et al., 2016). These fracture zones may also have facilitated the rise of magma. Moreover, as evidenced at Mount St Helens (e.g., Endo et al., 1981; Tilling et al., 1990; Lagmay et al., 2000) and in Ecuador (Andrade et al., 2018), fault activity may also favor sector collapses. It seems to have been the case for Huisla volcano, since the Pallatanga fault is roughly aligned with the orientation of its flank collapse amphitheater (Fig. 5b) that occurred between 215 and 180 ka (Table 1). In addition, the morphology of Mulmul volcano shows that its southeastern side is more eroded than Huisla volcano, even though Mulmul is much younger (Table 1). The dismantling of both edifices could have been promoted by a recent activity along these segments of the Pallatanga fault (Fig. 5b), triggering local collapses, thereby enhancing the effects of erosion and river incision. The gradual erosion of the banks of the deep Río Chambo valley could also have played a role in the dismantling of Mulmul's eastern flank.

Finally, the morphological comparison of the two largest edifices studied here, ***Sagoatoa*** and ***Igualata*** volcanoes, highlights the impact of the tectonic activity on erosion of volcanoes. Both volcanoes are located in the Interandean Valley. Sagoatoa volcano seems rather unaffected by tectonics, although no survey focused on the western edge of the Interandean Valley was performed, except south of Chimborazo (Baize et al., 2015). On the contrary, Igualata is cross-cut by the Pallatanga fault (Baize et al., 2016; Fig. 6), forming a sigmoidal graben-like structure in its central area. Such structure is characteristic of a locally extensive deformation, typical of interactions between strike-slip faults and volcanic edifices (Mathieu and van Wyk de Vries, 2011; Lagmay et al., 2000; Andrade et al., 2018). The different tectonic settings of Sagoatoa and Igualata volcanoes may thus influence their different erosional processes. A simple way to compare the degree of erosion affecting each volcano is to calculate the circularity index (Grosse et al., 2009, 2012) of a contour line located mid-height of the volcano. This index is defined by $C = \frac{4\pi A}{P2}$, with A being the area contained within the contour line and P its perimeter. C tends towards 1 for a quasi-circular line, which would characterize non-eroded flanks of a young edifice, while it gets closer to 0 for a highly eroded volcano. Circularity index of Sagoatoa volcano is ~0.34 for the contour line at 3480 m (unaffected by the presence of Pilisurco to the west), while the circularity index for Igualata is ~0.19 at 3770 m. Igualata volcano is thus much more eroded than Sagoatoa, despite the fact that it is only half the age. The presence of faults facilitated the erosion of volcanic edifices, more specifically by destroying the edifice during earthquakes, but also by driving water circulation (e.g., Traineau et al., 1989). The striking morphologic difference between Sagoatoa and Igualata volcanoes can thus be related to the impact of the shear of the Pallatanga fault on Igualata volcano, which favored erosion and led to the formation of the wide valleys observed in the present-day landscape. However, they could have experienced different climatic conditions that would increase the apparent tectonic impact on erosion, as Igualata volcano has a summit elevation that currently reaches 4430 m and could have been capped by a glacier during the Younger Dryas and/or Neoglacial periods (Clapperton, 1990; Samaniego et al., 2012), contrary to the Sagoatoa summit, which culminates at 4169 m and may not have experienced any glacial erosion since the LGM.

To summarize, our new ages suggest that the Pallatanga fault is active since at least ~350 ka, i.e. at the end of Igualata main edifice construction (Fig. 6c). It shows an ongoing activity, as evidenced by Huisla sector collapse that occurred at 215–180 ka, by Chimborazo collapse deposits that are sheared and present fault related pressure ridges (Baize et al., 2016) since at least ~62 ka (Fig. 6d), and by the distal Guano lava flow, displaced by the fault during the last 6 ka (Fig. 6d).

5.5. Geodynamical evolution of the Ecuadorian range in the last million years

The new ages provided in this study (Table 1) highlight the southward migration of the volcanic activity of the Ecuadorian arc since 600 ka (Figs. 6 and 7). It correlates with (1) a change of the position and orientation of the volcanic front (Fig. 7), (2) the geometry of the slab at depth and the presence of a flexure zone (Fig. 8), and (3) the activity of the Pallatanga fault segment of the CCPP fault system (Figs. 6 and 8). We interpret these interactions by proposing the following geodynamic scenario.

Since the beginning of the subduction of the Carnegie Ridge, which could have occurred between 15 and 1 Ma (e.g., Lonsdale and Klitgord, 1978; Spikings et al., 2001), coupling between the Nazca plate and South American continent increased (Spikings et al., 2001; Espurt et al., 2008; Nocquet et al., 2014). This strain accumulation intensifies at 3 to 6 Ma, contributing to the uplift of the Ecuadorian Andes and forearc basins (Spikings et al., 2001; Pedoja et al., 2006; Alvarado et al., 2016). The oblique convergence of the Nazca plate led to re-activation of N-S suture zones segments (Alvarado et al., 2016), progressively reorganized and connected with the more recent Pallatanga and Chingual oblique fault systems. While the dip of the subducting plate is too flat in Peru and Southern Ecuador to trigger partial melting of the mantle wedge (e.g., Gutscher et al., 1999), pressure and temperature conditions favored the magmatic production in the northern part of Ecuador, and the Quaternary volcanic arc developed in front of the Carnegie ridge (Fig. 7). The convex geometry of the margin, the presence of the over thickened Carnegie ridge, together with the stress increase related to its arrival in the trench area, lead to the formation of a major slab flexure at depth (Yepes et al., 2016), driven by the Grijalva fracture zone subduction (Fig. 8). Additionally, the detailed seismic tomography of Ecuador also evidences a curvature of the Mohorovičić discontinuity between 1 and 2°S (Araujo, 2013). Relative to the South American continent margin, and due to the oblique convergence, the location of this slab flexure slightly moved southward as the oceanic plate was subducted. The fast evolution of the slab depth, the width of the flexure and its slope, may have initialized the migration of the volcanic arc for the last 600 ka. Moreover, as the arc magmatism occurred above the subducting plate from a rather constant depth, between 90 and 120 km in Ecuador (Fig. 8), the location and orientation of the volcanic front changed markedly, from ~27°NE to ~320°NW, following the new orientation of the slab at depth. Finally, the activity of major faults and the presence of suture zones (Alvarado et al., 2016) favored magma ascent and participated in the important development of the arc since 400–300 ka (Fig. 7). In parallel, magmatic dikes and sporadic intrusion of magma through crustal faults may have also contributed to the development of the Chingual-Cosanga-Pallatanga-Puná (CCPP) fault system activity, which remains very active today (Winter et al., 1993; Tibaldi et al., 2007; Alvarado et al., 2014; Baize et al., 2015; Alvarado et al., 2016; Champenois et al., 2017).

Along the American Pacific coast, several areas are characterized by the subduction of an aseismic ridge, such as the Cocos ridge in Central America, the Nazca ridge and the Inca Plateau in Peru, and the Juan-Fernandez ridge in Chile (e.g., Espurt et al., 2008). However, the influence of these ridges on geodynamics is variable. Indeed, at these three locations the geometry of the slab is rather flat due to a higher buoyancy of the oceanic crust (e.g., Pilger, 1984; Gutscher et al., 2000), while the Nazca plate presents a deep flexure below Ecuador. This can

be related to the age, and therefore density difference of the subducting oceanic crust across the Grijalva fracture zone. In addition, the flat slab of Mexico does not prevent the development of a Quaternary volcanic arc, contrary to Peru and Chile, where no recent volcanism is present (e.g., Manea et al., 2017). Gutscher et al. (2000) suggest that volcanism can occur during the early stages of a flat subduction, and wane progressively with the lack of mantle wedge and a prolonged cooling of the subducting lithosphere. Following this hypothesis, the present geodynamic setting of Ecuador would be at an early stage of the slab geometry evolution, preceding a long-term shallowing of the Nazca plate and a gradual decrease of volcanism in the far future (Gutscher et al., 2000; Espurt et al., 2008; Ramos and Folguera, 2009).

6. Conclusions

The twenty-five new K-Ar ages performed on groundmass for young volcanic activity characterization presented in this study provide new temporal constraints on the development of the Ecuadorian arc. Although the periods of activity of some volcanoes remain poorly documented at the regional scale, such as Sangay, Altar or Pilisurco, edifices from the southern termination of the arc appear significantly younger than northern volcanoes (Samaniego et al., 2005; Opdyke et al., 2006; Hidalgo et al., 2008; Hoffer, 2008; Robin et al., 2010; Alvarado et al., 2014). An intensification of the volcanic activity seems to have occurred since 600 ka, with the construction of Huisla, Igualata, Sangay (Monzier et al., 1999b), Tungurahua (Hall et al., 1999; Le Pennec et al., 2006; Bablon et al., 2018a), then Carihuairazo, Chimborazo (Samaniego et al., 2012) and Mulmul volcanoes, in the vicinity of the Pallatanga fault. In addition, the magmatic composition of most recent strombolian cones, such as those of Calpi, Licto and Puñalica, contrasts with the rest of the arc by showing a more primitive signature. We attribute the southward migration of volcanism to a recent reorganization of the geodynamic context of Ecuador, linked to the oblique convergence of the Nazca plate, and both Grijalva fracture zone and Carnegie Ridge subduction. The coupling between the subducting plate and the South American continent, intensified with the increase of crustal material accumulating into the trench and the oceanic crust age difference across the Grijalva fracture zone, triggered the formation of a slab flexure at depth (Yepes et al., 2016). Strains were accommodated at the surface by the activation of the major CCPP fault system. Moreover, the new ages allow us to estimate that the Pallatanga fault was active since at least 350 ka, with a displacement velocity of about 3.3 to 10 $mm{\cdot}a^{-1}$ since the last 6 ka. Our hypothesis relating volcanic arc development in direct connection with the upper plate and slab geodynamics in Ecuador seems to favor a future increase of the number of volcanoes to the south of the current active arc.

Acknowledgments

The authors warmly thank Victor Ramos and an anonymous reviewer for their constructive comments and detailed reviews that greatly improved this manuscript. We thank members of Instituto Geofísico (Escuela Politécnica Nacional) of Quito for their support during field trips, and the French Institut de Recherche pour le Développement (IRD), through the Laboratoire Mixte International program “Séismes et Volcans dans les Andes du Nord”, which made this work possible. We also wish to thank Valérie Godard for her quality manufacturing of the thin sections, Fanny Soler for her help during preparations and measurements of Sagoatoa, Calpi and Guano samples, as well as Santiago Santamaría for useful discussions, Pierre Lahitte for his advices and remarks concerning the impact of erosion on the morphology, and Sébastien Lénard for his suggestions on the earlier draft of the manuscript. This work is dedicated to the memory of our colleague Michel Monzier, volcanologist at IRD, which was the first to describe the unusual characteristic of the southern termination of the Ecuadorian arc. This publication was financially supported by CNRS-INSU TelluS Aleas (INSU 2015-ALEAS) and LMI-IRD (2012-16 LMI-SVAN-IRD) programs. This is LGMT contribution number 150 and Laboratory of Excellence ClerVolc contribution number 323.

Appendix A. Supplementary data

Supplementary data associated with this article can be found in the online version, at https://doi.org/10.1016/j.tecto.2018.12.010. These data include the Google map of the most important areas described in this article.

References

Alvarado, A., Audin, L., Nocquet, J.M., Lagreulet, S., Segovia, M., Font, Y., Lamarque, G., Yepes, H., Mothes, P., Rolandone, F., Jarrín, P., Quidelleur, X., 2014. Active tectonics in Quito, Ecuador, assessed by geomorphological studies, GPS data, and crustal seismicity. Tectonics 33, 67–83. https://doi.org/10.1002/2012TC003224.

Alvarado, A., Audin, L., Nocquet, J.M., Jaillard, E., Mothes, P., Jarrín, P., Segovia, M., Rolandone, F., Cisneros, D., 2016. Partitioning of oblique convergence in the Northern Andes subduction zone: migration history and the present-day boundary of the North Andean Sliver in Ecuador. Tectonics 35, 1048–1065. https://doi.org/10.1002/2016TC004117.

Ancellin, M.-A., Samaniego, P., Vlastélic, I., Nauret, F., Gannoun, A., Hidalgo, S., 2017. Across-arc versus along-arc Sr-Nd-Pb isotope variations in the Ecuadorian volcanic arc. Geochem. Geophys. Geosyst. 18, 1163–1188. https://doi.org/10.1002/2016GC006679.

Andrade, S.D., van Wyk de Vries, B., Robin, C., 2018. Imbabura volcano (Ecuador): the influence of dipping-substrata on the structural development of composite volcanoes during strike-slip faulting. J. Volcanol. Geotherm. Res. https://doi.org/10.1016/j.jvolgeores.2018.11.017. (In press).

Araujo, S., 2013. The Ecuadorian moho. In: La Granja, Revista de Ciencias de la Vida. 18 (2). Universidad Politécnica Salesiana, Ecuador, pp. 43–47.

Aspden, J.A., McCourt, W.J., Brook, M., 1987. Geometrical control of subduction-related magmatism: the Mesozoic and Cenozoic plutonic history of Western Colombia. J. Geol. Soc. 144, 893–905.

Bablon, M., Quidelleur, X., Samaniego, P., Le Pennec, J.-L., Lahitte, P., Liorzou, C., Bustillos, J.E., Hidalgo, S., 2018a. Eruptive chronology of Tungurahua volcano (Ecuador) revisited based on new K Ar ages and geomorphological reconstructions. J. Volcanol. Geotherm. Res. 357, 378–398. https://doi.org/10.1016/j.jvolgeores.2018.05.007.

Bablon, M., Quidelleur, X., Samaniego, P., Le Pennec, S., Hidalgo, 2018b. New unspiked K-Ar ages of Holocene lava flows and pumices from the Ecuadorian arc. In: Cities on Volcanoes. vol. 10. Naples, Italy, pp. 637.

Baize, S., Audin, L., Winter, T., Alvarado, A., Pilatasig Moreno, L., Taipe, M., Reyes, P., Kauffmann, P., Yepes, H., 2015. Paleoseismology and tectonic geomorphology of the Pallatanga fault (Central Ecuador), a major structure of the South-American crust. Geomorphology 237, 14–28. https://doi.org/10.1016/j.geomorph.2014.02.030.

Baize, S., Audin, L., Alvarado, A., Champenois, J., 2016. Earthquake fault segmentation in the Central Andes, Ecuador. In: Extended Abstract, 7th International INQUA Meeting on Paleoseismology, Active Tectonics and Archaeoseismology, Crestone, Colorado, USA.

Barba, D., Robin, C., Samaniego, P., Eissen, J.-P., 2008. Holocene recurrent explosive activity at Chimborazo volcano (Ecuador). J. Volcanol. Geotherm. Res. 176, 27–35. https://doi.org/10.1016/j.jvolgeores.2008.05.004.

Barberi, F., Coltelli, M., Ferrara, G., Innocenti, F., Navarro, J.M., Santacroce, R., 1988. Plio-Quaternary volcanism in Ecuador. Geochem. Mag. 125, 1–14.

Barragán, R., Geist, D., Hall, M., Larson, P., Kurz, M., 1998. Subduction controls on the compositions of lavas from the Ecuadorian Andes. Earth Planet. Sci. Lett. 154, 153–166. https://doi.org/10.1016/S0012821X(97)00141-6.

Barragán, R., Baby, P., Duncan, R., 2005. Cretaceous alkaline intra-plate magmatism in the Ecuadorian Oriente Basin: Geochemical, geochronological and tectonic evidence. Earth Planet. Sci. Lett. 236, 670–690. https://doi.org/10.1016/j.epsl.2005.03.016.

Beate, B., Hammersley, L., DePaolo, D., Deino, A.I., 2006. La Edad de la Ignimbrita de Chalupas, Prov. De Cotopaxi, Ecuador, y su importancia como marcador estratigráfico. In: 6th Jornadas en Ciencias de la Tierra. EPN, Quito, pp. 68–71.

Béguelin, P., Chiaradia, M., Beate, B., Spikings, R., 2015. The Yanaurcu volcano (Western Cordillera, Ecuador): a field, petrographic, geochemical, isotopic and geochronological study. Lithos 218–219, 37–53. https://doi.org/10.1016/j.lithos.2015.01.014.

Bernard, B., Andrade, D., 2011. Volcanes Cuaternarios del Ecuador Continental. Map 1:500000.

Bernard, B., van Wyk de Vries, B., Barba, D., Leyrit, H., Robin, C., Alcaraz, S., Samaniego, P., 2008. The Chimborazo sector collapse and debris avalanche: Deposit characteristics as evidence of emplacement mechanisms. J. Volcanol. Geotherm. Res. 176, 36–43. https://doi.org/10.1016/j.jvolgeores.2008.03.012.

Bernard, B., Hidalgo, S., Robin, C., Beate, B., Quijozaca, J., 2014. The 3640–3510 BC rhyodacite eruption of Chachimbiro compound volcano, Ecuador: a violent directed blast produced by a satellite dome. Bull. Volcanol. 76. https://doi.org/10.1007/s00445-014-0849-z.

Bird, P., 2003. An updated digital model of plate boundaries. Geochem. Geophys. Geosyst. 4 (3). https://doi.org/10.1029/2001GC000252.

Bryant, J.A., Yogodzinski, G.M., Hall, M.L., Lewicki, J.L., Bailey, D.G., 2006. Geochemical constraints on the origin of volcanic rocks from the Andean Northern Volcanic Zone,

Ecuador. J. Petrol. 47, 1147–1175. https://doi.org/10.1093/petrology/egl006.
Bustillos, J.E., 2008. Las avalanchas de escombros en el sector del volcán Tungurahua. Facultad de ingeniería en geología y petróleos, Escuela Politécnica Nacional, Quito.
Cassignol, C., Gillot, P.-Y., 1982. Range and effectiveness of unspiked potassium-argon dating: experimental groundwork and application. In: Odin GS Ed Numer. Dating Stratigr. John Wiley & Sons, New York, pp. 159–179.
Champenois, J., Baize, S., Vallée, M., Jomard, H., Alvarado, A., Espin, P., Ekstrom, G., Audin, L., 2017. Evidences of surface rupture associated with a low magnitude (Mw5.0) shallow earthquake in the Ecuadorian Andes: Andean earthquake surface rupture. J. Geophys. Res. Solid Earth. https://doi.org/10.1002/2017JB013928.
Clapperton, C.M., 1990. Glacial and volcanic geomorphology of the Chimborazo-Carihuairazo Massif, Ecuadorian Andes. Trans. R. Soc. Edinb. Earth Sci. 81, 91–116.
Collot, J.-Y., Michaud, F., Alvarado, A., Marcaillou, B., Sosson, M., Ratzov, G., Migeon, S., Calahorrano, A., Pazmino, A., 2009. Visión general de la morfología submarina del margen convergente de Ecuador-Sur de Colombia: implicaciones sobre la transferencia de masa y la edad de la subducción de la Cordillera de Carnegie, Primera Edición. Comisión Nacional del Derecho del Mar (CNDM), pp. 47–74.
Coltorti, M., Ollier, C.D., 2000. Geomorphic and tectonic evolution of the Ecuadorian Andes. Geomorphology 32, 1–19.
Cotten, J., Le Dez, A., Bau, M., Caroff, M., Maury, R.C., Dulski, P., Fourcade, S., Bohn, M., Brousse, R., 1995. Origin of anomalous rare-earth element and yttrium enrichments in subaerially exposed basalts: evidence from French Polynesia. Chem. Geol. 119, 115–138.
DeMets, C., Gordon, R.G., Argus, D.F., 2010. Geologically current plate motions. Geophys. J. Int. 181, 1–80. https://doi.org/10.1111/j.1365-246X.2009.04491.x.
Deniaud, Y., Baby, P., Basile, C., Ordoñez, M., Montenegro, G., Mascle, G., 1999. Opening and tectonic and sedimentary evolution of the Gulf of Guayaquil: Neogene and Quaternary fore-arc basin of the south Ecuadorian Andes. Comptes Rendus de l'Académie des Sciences - Series IIA. Earth Planet. Sci. Lett. 328, 181–187.
Dumont, J.F., Santana, E., Vilema, W., Pedoja, K., Ordóñez, M., Cruz, M., Jiménez, N., Zambrano, I., 2005. Morphological and microtectonic analysis of Quaternary deformation from Puná and Santa Clara Islands, Gulf of Guayaquil, Ecuador (South America). Tectonophysics 399, 331–350. https://doi.org/10.1016/j.tecto.2004.12.029.
Egbue, O., Kellogg, J., 2010. Pleistocene to present North Andean "escape". Tectonophysics 489, 248–257. https://doi.org/10.1016/j.tecto.2010.04.021.
Ego, F., Sébrier, M., Lavenu, A., Yepes, H., Egues, A., 1996. Quaternary state of stress in the Northern Andes and the restraining bend model for the Ecuadorian Andes. Tectonophysics 259, 101–116.
Endo, E.T., Malone, S.D., Noson, L.L., Weaver, C.S., 1981. Locations, magnitudes and statistics of the March 20-May 18 earthquake sequence. In: The 1980 eruptions of Mount St. Helens, Washington, U. S. Geol. Surv. Profess. Paper 1250, pp. 93–107.
England, P., Engdahl, R., Thatcher, W., 2004. Systematic variation in the depths of slabs beneath arc volcanoes. Geophys. J. Int. 156, 377–408. https://doi.org/10.1111/j.1365-246X.2003.02132.x.
Espín, P.A., 2014. Caracterización geológica y litológica de los depósitos laháricos de Mera, provincia de Pastaza. Facultad de Geología y Petróleos, Escuela Politécnica Nacional, Quito.
Espín, P.A., Mothes, P.A., Hall, M.L., Valverde, V., Keen, H., 2018. The "Mera" lahar deposit in the upper Amazon basin: Transformation of a late Pleistocene collapse at Huisla volcano, Central Ecuador. J. Volcanol. Geotherm. Res. https://doi.org/10.1016/j.jvolgeores.2018.10.008.
Espurt, N., Funiciello, F., Martinod, J., Guillaume, B., Regard, V., Faccenna, C., Brusset, S., 2008. Flat subduction dynamics and deformation of the South American plate: Insights from analog modeling. Tectonics 27, TC3011. https://doi.org/10.1029/2007TC002175.
Germa, A., Quidelleur, X., Gillot, P.Y., Tchilinguirian, P., 2010. Volcanic evolution of the back-arc Pleistocene Payun Matru volcanic field (Argentina). J. S. Am. Earth Sci. 29, 717–730. https://doi.org/10.1016/j.jsames.2010.01.002.
Germa, A., Quidelleur, X., Lahitte, P., Labanieh, S., Chauvel, C., 2011. The K–Ar Cassignol–Gillot technique applied to western Martinique lavas: a record of Lesser Antilles arc activity from 2 Ma to Mount Pelée volcanism. Quat. Geochronol. 6, 341–355. https://doi.org/10.1016/j.quageo.2011.02.001.
Gillot, P.-Y., Hildenbrand, A., Lefèvre, J.-C., Albore-Livadie, C., 2006. The K/Ar dating method: principle, analytical techniques, and application to Holocene volcanic eruptions in Southern Italy. Acta Vulcanol. 18, 55–66.
Graindorge, D., Calahorrano, A., Charvis, P., Collot, J.-Y., Bethoux, N., 2004. Deep structures of the Ecuador convergent margin and the Carnegie Ridge, possible consequence on great earthquakes recurrence interval. Geophys. Res. Lett. 31. https://doi.org/10.1029/2003GL018803.
Grosse, P., van Wyk de Vries, B., Petrivonic, I.A., Euillades, P.A., Alvarado, G.E., 2009. Morphometry and evolution of arc volcanoes. Geology 37, 651–654. https://doi.org/10.1130/G25734A.1.
Grosse, P., van Wyk de Vries, B., Euillades, P.A., Kervyn, M., Petrinovic, I.A., 2012. Systematic morphometric characterization of volcanic edifices using digital elevation models. Geomorphology 136, 114–131. https://doi.org/10.1016/j.geomorph.2011.06.001.
Guillier, B., Chatelain, J.-L., Jaillard, E., Yepes, H., Poupinet, G., Fels, J.-F., 2001. Seismological evidence on the geometry of the orogenic system in Central-Northern Ecuador (South America). Geophys. Res. Lett. 28, 3749–3752.
Gutscher, M.-A., Malavieille, J., Lallemand, S., Collot, J.-Y., 1999. Tectonic segmentation of the North Andean margin: impact of the Carnegie Ridge collision. Earth Planet. Sci. Lett. 168, 255–270.
Gutscher, M.-A., Maury, R., Eissen, J.-P., Bourdon, E., 2000. Can slab melting be caused by flat subduction? Geology 28, 535–538.
Hall, M.L., Beate, B., 1991. El Volcanism o Plio-Cuaternario en los Andes del Ecuador. In: El Paisaje Volcánico de la Sierra Ecuatoriana. Corp. Edit. Nac., Quito, pp. 5–18.
Hall, M.L., Mothes, P.A., 2008. Quilotoa volcano - Ecuador: an overview of young dacitic volcanism in a lake-filled caldera. J. Volcanol. Geotherm. Res. 176, 44–55. https://doi.org/10.1016/j.jvolgeores.2008.01.025.
Hall, M.L., Wood, C.A., 1985. Volcano-tectonic segmentation of the northern Andes. Geology 13, 203–207.
Hall, M.L., Robin, C., Beate, B., Mothes, P., Monzier, M., 1999. Tungurahua Volcano, Ecuador: structure, eruptive history and hazards. J. Volcanol. Geotherm. Res. 91, 1–21.
Hall, M.L., Samaniego, P., Le Pennec, J.L., Johnson, J.B., 2008. Ecuadorian Andes volcanism: a review of Late Pliocene to present activity. J. Volcanol. Geotherm. Res. 176, 1–6. https://doi.org/10.1016/j.jvolgeores.2008.06.012.
Hall, M.L., Mothes, P.A., Samaniego, P., Militzer, A., Beate, B., Ramón, P., Robin, C., 2017. Antisana volcano: a representative andesitic volcano of the eastern cordillera of Ecuador: petrography, chemistry, tephra and glacial stratigraphy. J. S. Am. Earth Sci. 73, 50–64. https://doi.org/10.1016/j.jsames.2016.11.005.
Hampel, A., 2002. The migration history of the Nazca Ridge along the Peruvian active margin: a re-evaluation. Earth Planet. Sci. Lett. 203, 665–679.
Harford, C.L., Pringle, M.S., Sparks, R.S.J., Young, S.R., 2002. The volcanic evolution of Montserrat using $^{40}Ar/^{39}Ar$ geochronology. Geol. Soc. Lond. Mem. 21, 93–113. https://doi.org/10.1144/GSL.MEM.2002.021.01.05.
Hayes, G.P., Wald, D.J., Johnson, R.L., 2012. Slab1.0: A three-dimensional model of global subduction zone geometries. J. Geophys. Res. Solid Earth 117, B01302. https://doi.org/10.1029/2011JB008524.
Hey, R., 1977. Tectonic evolution of the Cocos-Nazca spreading center. Geol. Soc. Am. Bull. 88, 1404–1420.
Hidalgo, S., 2006. Les interactions entre magmas calco-alcalins "classiques" et adakitiques: exemple du complexe volcanique Atacazo-Ninahuilca (Equateur). Université Blaise Pascal, Clermont-Ferrand II.
Hidalgo, S., Monzier, M., Almeida, E., Chazot, G., Eissen, J.-P., van der Plicht, J., Hall, M.L., 2008. Late Pleistocene and Holocene activity of the Atacazo–Ninahuilca Volcanic complex (Ecuador). J. Volcanol. Geotherm. Res. 176, 16–26. https://doi.org/10.1016/j.jvolgeores.2008.05.017.
Hidalgo, S., Gerbe, M.C., Martin, H., Samaniego, P., Bourdon, E., 2012. Role of crustal and slab components in the Northern Volcanic Zone of the Andes (Ecuador) constrained by Sr–Nd–O isotopes. Lithos 132–133, 180–192. https://doi.org/10.1016/j.lithos.2011.11.019.
Hoffer, G., 2008. Fusion partielle d'un manteau métasomatisé par un liquide adakitique: approches géochimique et expérimentale de la genèse et de l'évolution des magmas de l'arrière-arc équatorien. Université Blaise Pascal, Clermont-Ferrand II.
Hoffer, G., Eissen, J.-P., Beate, B., Bourdon, E., Fornari, M., Cotten, J., 2008. Geochemical and petrological constraints on rear-arc magma genesis processes in Ecuador: the Puyo cones and Mera lavas volcanic formations. J. Volcanol. Geotherm. Res. 176, 107–118. https://doi.org/10.1016/j.jvolgeores.2008.05.023.
Hughes, R.A., Pilatasig, L.F., 2002. Cretaceous and Tertiary terrane accretion in the Cordillera Occidental of the Andes of Ecuador. Tectonophysics 345, 29–48.
Jaillard, E., Bengtson, P., Ordoñez, M., Vaca, W., Dhondt, A., Suárez, J., Toro, J., 2008. Sedimentary record of terminal cretaceous accretions in Ecuador: the Yunguilla Group in the Cuenca area. J. S. Am. Earth Sci. 25, 133–144. https://doi.org/10.1016/j.jsames.2007.08.002.
Jaillard, E., Lapierre, H., Ordonez, M., Alava, J.T., Amortegui, A., Vanmelle, J., 2009. Accreted oceanic terranes in Ecuador: southern edge of the Caribbean Plate? Geol. Soc. Lond. Spec. Publ. 328, 469–485. https://doi.org/10.1144/SP328.19.
James, D.E., 1971. Plate tectonic model for the evolution of the Central Andes. Geol. Soc. Am. Bull. 82, 3325–3346.
Kellogg, J.N., Vega, V., 1995. Tectonic development of Panama, Costa Rica, and the Colombian Andes: Constraints from Global Positioning System geodetic studies and gravity. In: Mann, P. (Ed.), Geologic and Tectonic Development of the Caribbean Plate Boundary in Southern Central America. Geological Society of America Special Paper, Boulder, Colorado, pp. 295.
Kendrick, E., Bevis, M., Smalley, R., Brooks, B., Vargas, R.B., Lauría, E., Fortes, L.P.S., 2003. The Nazca–South America Euler vector and its rate of change. J. S. Am. Earth Sci. 16, 125–131. https://doi.org/10.1016/S0895-9811(03)00028-2.
Kerr, A.C., Aspden, J.A., Tarney, J., Pilatasig, L.F., 2002. The nature and provenance of accreted oceanic terranes in western Ecuador: geochemical and tectonic constraints. J. Geol. Soc. 159, 577–594. https://doi.org/10.1144/0016-764901-151.
Lagmay, A.M.F., van Wyk de Vries, B., Kerle, N., Pyle, D.M., 2000. Volcano instability induced by strike-slip faulting. Bull. Volcanol. 62, 331–346. https://doi.org/10.1007/s004450000103.
Lavenu, A., Noblet, C., Bonhomme, M.G., Egüez, A., Dugas, F., Vivier, G., 1992. New K-Ar age dates of Neogene and Quaternary volcanic rocks from the Ecuadorian Andes: Implications for the relationship between sedimentation, volcanism, and tectonics. J. S. Am. Earth Sci. 5, 309–320.
Lavenu, A., Winter, T., Dávila, F., 1995. A Pliocene–Quaternary compressional basin in the Interandean Depression, Central Ecuador. Geophys. J. Int. 121, 279–300. https://doi.org/10.1111/j.1365246X.1995.tb03527.x.
Le Pennec, J.-L., Hall, M.L., Robin, C., Bartomioli, E., 2006. Tungurahua volcano, Late Holocene activity. In: Fourth Conference Cities on Volcanoes. IAVCEI, Quito (Ecuador).
Le Pennec, J.L., Ruiz, A.G., Eissen, J.P., Hall, M.L., Fornari, M., 2011. Identifying potentially active volcanoes in the Andes: Radiometric evidence for late Pleistocene-early Holocene eruptions at Volcán Imbabura, Ecuador. J. Volcanol. Geotherm. Res. 206, 121–135. https://doi.org/10.1016/j.jvolgeores.2011.06.002.
Le Pennec, J.-L., De Saulieu, G., Samaniego, P., Jaya, D., Gailler, L., 2013. A devastating plinian eruption at Tungurahua Volcano reveals formative occupation at 1100 cal BC in Central Ecuador. Radiocarbon 55, 1199–1214.

Litherland, M., Aspden, J.A., Egüez, A., 1993. Mapa geológico de la República del Ecuador 1:1000000. British Geological Survey y CODIGEM.
Lonsdale, P., 2005. Creation of the Cocos and Nazca plates by fission of the Farallon plate. Tectonophysics 404, 237–264. https://doi.org/10.1016/j.tecto.2005.05.011.
Lonsdale, P., Klitgord, K.D., 1978. Structure and tectonic history of the eastern Panama Basin. Geol. Soc. Am. Bull. 89, 981–999.
Manea, V.C., Manea, M., Ferrari, L., Orozco-Esquivel, T., Valenzuela, R.W., Husker, A., Kostoglodov, V., 2017. A review of the geodynamic evolution of flat slab subduction in Mexico, Peru, and Chile. Tectonophysics 695, 27–52. https://doi.org/10.1016/j.tecto.2016.11.037.
Mathieu, L., van Wyk de Vries, B., 2011. The impact of strike-slip, transtensional and transpressional fault zones on volcanoes. Part 1: Scaled experiments. J. Struct. Geol. 33, 907–917. https://doi.org/10.1016/j.jsg.2011.03.002.
Meschede, M., Barckhausen, U., 2001. The relationship of the Cocos and Carnegie ridges: age constraints from paleogeographic reconstructions. Int. J. Earth Sci. 90, 386–392. https://doi.org/10.1007/s005310000155.
Monzier, M., Robin, C., Hall, M.L., Cotten, J., Samaniego, P., 1999a. Geochemistry and Tectonics at the Southern Termination of the Northern Volcanic Zone (Riobamba Volcanoes, Ecuador): Preliminary Results. Fourth ISAG, Goettingen (Germany), pp. 516–518.
Monzier, M., Robin, C., Samaniego, P., Hall, M.L., Cotten, J., Mothes, P., Arnaud, N., 1999b. Sangay volcano, Ecuador: structural development, present activity and petrology. J. Volcanol. Geotherm. Res. 90, 49–79.
Narvaez, D.F., Rose-Koga, E.F., Samaniego, P., Koga, K.T., Hidalgo, S., 2018. Constraining magma sources using primitive olivine-hosted melt inclusions from Puñalica and Sangay volcanoes (Ecuador). Contrib. Mineral. Petrol. 173 (10). https://doi.org/10.1007/s00410-018-1508-8.
Nocquet, J.-M., Villegas-Lanza, J.C., Chlieh, M., Mothes, P.A., Rolandone, F., Jarrin, P., Cisneros, D., Alvarado, A., Audin, L., Bondoux, F., Martin, X., Font, Y., Régnier, M., Vallée, M., Tran, T., Beauval, C., Maguiña Mendoza, J.M., Martinez, W., Tavera, H., Yepes, H., 2014. Motion of continental slivers and creeping subduction in the northern Andes. Nat. Geosci. 7, 287–291. https://doi.org/10.1038/ngeo2099.
Opdyke, N.D., Hall, M., Mejia, V., Huang, K., Foster, D.A., 2006. Time-averaged field at the equator: results from Ecuador. Geochem. Geophys. Geosyst. 7. https://doi.org/10.1029/2005GC001221.
Ordóñez, J., 2012. Depósitos volcánicos del Pleistoceno Tardío en la cuenca de. In: Ambato: caracterización, distribución y origen. Quito, Escuela Politécnica Nacional.
Peccerillo, A., Taylor, S.R., 1976. Geochemistry of Eocene calc-alkaline volcanic rocks from the Kastamonu area, northern Turkey. Contrib. Mineral. Petrol. 58, 63–81.
Pedoja, K., Dumont, J.F., Lamothe, M., Ortlieb, L., Collot, J.-Y., Ghaleb, B., Auclair, M., Alvarez, V., Labrousse, B., 2006. Plio-Quaternary uplift of the Manta Peninsula and La Plata Island and the subduction of the Carnegie Ridge, central coast of Ecuador. J. S. Am. Earth Sci. 22, 1–21. https://doi.org/10.1016/j.jsames.2006.08.003.
Pennington, W.D., 1981. Subduction of the Eastern Panama Basin and seismotectonics of northwestern South America. J. Geophys. Res. 86, 10753–10770.
Pilger, R.H., 1984. Cenozoic plate kinematics, subduction and magmatism: South American Andes. J. Geol. Soc. 141, 793–802.
Ramos, V., Folguera, A., 2005. Tectonic evolution of the Andes of Neuquén: Constraints derived from the magmatic arc and foreland deformation. In: Veiga, G., Spalletti, L., Howell, J., Schwarz, E. (Eds.), The Neuquén Basin: A Case Study in Sequence Stratigraphy and Basin Dynamics. Geol. Soc. Lond. Spec. Publ. 252, pp. 15–35.
Ramos, V.A., Folguera, A., 2009. Andean flat-slab subduction through time. Geol. Soc. Lond. Spec. Publ. 327, 31–54. https://doi.org/10.1144/SP327.3.
Ricci, J., Quidelleur, X., Lahitte, P., 2015. Volcanic evolution of Central Basse-Terre Island revisited on the basis of new geochronology and geomorphology data. Bull. Volcanol. 77. https://doi.org/10.1007/s00445015-0970-7.
Robin, C., Samaniego, P., Le Pennec, J.-L., Fornari, M., Mothes, P., van der Plicht, J., 2010. New radiometric and petrological constraints on the evolution of the Pichincha volcanic complex (Ecuador). Bull. Volcanol. 72, 1109–1129. https://doi.org/10.1007/s00445-010-0389-0.
Sallarès, V., Charvis, P., 2003. Crustal thickness constraints on the geodynamic evolution of the Galapagos Volcanic Province. Earth Planet. Sci. Lett. 214, 545–559. https://doi.org/10.1016/S0012-821X(03)00373-X.
Samaniego, P., Monzier, M., Robin, C., Hall, M.L., 1998. Late Holocene eruptive activity at Nevado Cayambe Volcano, Ecuador. Bull. Volcanol. 59, 451–459.
Samaniego, P., Martin, H., Monzier, M., Robin, C., Fornari, M., Eissen, J.-P., Cotten, J., 2005. Temporal Evolution of Magmatism in the Northern Volcanic Zone of the Andes: the Geology and Petrology of Cayambe Volcanic complex (Ecuador). J. Petrol. 46, 2225–2252. https://doi.org/10.1093/petrology/egi053.
Samaniego, P., Robin, C., Chazot, G., Bourdon, E., Cotten, J., 2010. Evolving metasomatic agent in the Northern Andean subduction zone, deduced from magma composition of the long-lived Pichincha volcanic complex (Ecuador). Contrib. Mineral. Petrol. 160, 239–260. https://doi.org/10.1007/s00410-009-0475-5.
Samaniego, P., Le Pennec, J.-L., Robin, C., Hidalgo, S., 2011. Petrological analysis of the pre-eruptive magmatic process prior to the 2006 explosive eruptions at Tungurahua volcano (Ecuador). J. Volcanol. Geotherm. Res. 199, 69–84. https://doi.org/10.1016/j.jvolgeores.2010.10.010.
Samaniego, P., Barba, D., Robin, C., Fornari, M., Bernard, B., 2012. Eruptive history of Chimborazo volcano (Ecuador): a large, ice-capped and hazardous compound volcano in the Northern Andes. J. Volcanol. Geotherm. Res. 221–222, 33–51. https://doi.org/10.1016/j.jvolgeores.2012.01.014.
Samper, A., Quidelleur, X., Boudon, G., Le Friant, A., Komorowski, J.C., 2008. Radiometric dating of three large volume flank collapses in the Lesser Antilles Arc. J. Volcanol. Geotherm. Res. 176, 485–492. https://doi.org/10.1016/j.jvolgeores.2008.04.018.
Samper, A., Quidelleur, X., Komorowski, J.-C., Lahitte, P., Boudon, G., 2009. Effusive history of the Grande Découverte Volcanic complex, southern Basse-Terre (Guadeloupe, French West Indies) from new K–Ar Cassignol–Gillot ages. J. Volcanol. Geotherm. Res. 187, 117–130. https://doi.org/10.1016/j.jvolgeores.2009.08.016.
Schiano, P., Monzier, M., Eissen, J.-P., Martin, H., Koga, K.T., 2010. Simple mixing as the major control of the evolution of volcanic suites in the Ecuadorian Andes. Contrib. Mineral. Petrol. 160, 297–312. https://doi.org/10.1007/s00410-009-0478-2.
Smith, W.H.F., Sandwell, D.T., 1997. Global sea floor topography from satellite altimetry and ship depth soundings. Science 277, 1956–1962.
Spikings, R.A., Winkler, W., Seward, D., Handler, R., 2001. Along-strike variations in the thermal and tectonic response of the continental Ecuadorian Andes to the collision with heterogeneous oceanic crust. Earth Planet. Sci. Lett. 186, 57–73.
Steiger, R.H., Jäger, E., 1977. Subcommission on geochronology: convention on the use of decay constants in geo- and cosmochronology. Earth Planet. Sci. Lett. 36, 359–362.
Stübel A., Las montañas volcánicas del Ecuador: retratadas y descritas geológica-topográficamente, 2004, Banco Central del Ecuador; Quito. ISBN: 9978-43-567-0, reissue of 1897.
Sun, S.-s., McDonough, W.F., 1989. Chemical and isotopic systematics of oceanic basalts: implications for mantle composition and processes. Geol. Soc. Lond. Spec. Publ. 42, 313–345. https://doi.org/10.1144/GSL.SP.1989.042.01.19.
Syracuse, E.M., Abers, G.A., 2006. Global compilation of variations in slab depth beneath arc volcanoes and implications. Geochem. Geophys. Geosyst. 7. https://doi.org/10.1029/2005GC001045.
Tamura, Y., Tatsumi, Y., Zhao, D., Kido, Y., Shukuno, H., 2002. Hot fingers in the mantle wedge: new insights into magma genesis in subduction zones. Earth Planet. Sci. Lett. 197, 105–116.
Tatsumi, Y., 1986. Formation of the volcanic front in subduction zones. Geophys. Res. Lett. 13, 717–720.
Taylor, J.R., 1997. Introduction to Error Analysis, the Study of Uncertainties in Physical Measurements, 2nd edition. University Science Books.
Tibaldi, A., Rovida, A., Corazzato, C., 2007. Late Quaternary kinematics, slip-rate and segmentation of a major Cordillera-parallel transcurrent fault: the Cayambe-Afiladores-Sibundoy system, NW South America. J. Struct. Geol. 29, 664–680. https://doi.org/10.1016/j.jsg.2006.11.008.
Tilling, R.I., Topinka, L., Swanson, D.A., 1990. Eruptions of Mount St. Helens: past, present, and future. In: The Climactic Eruption of May 18, 1980. U.S. Geological Survey Special Interest Publication.
Traineau, H., Westercamp, D., Benderitter, Y., 1989. Case study of a volcanic geothermal system, Mount Pelée, Martinique. J. Volcanol. Geotherm. Res. 38, 49–66.
Trenkamp, R., Kellogg, J.N., Freymueller, J.T., Mora, H.P., 2002. Wide plate margin deformation, southern Central America and northwestern South America, CASA GPS observations. J. S. Am. Earth Sci. 15, 157–171.
Valverde, V., 2014. Las avalanchas de escombros provenientes del volcán Sangay: caracterización petrográfica-geoquímica. Escuela Politécnica Nacional, Quito.
Winter, T., Avouac, J.P., Lavenu, A., 1993. Late Quaternary kinematics of the Pallatanga strike-slip fault (Central Ecuador) from topographic measurements of displaced morphological features. Geophys. J. Int. 115, 905–920.
Witt, C., Bourgois, J., Michaud, F., Ordoñez, M., Jiménez, N., Sosson, M., 2006. Development of the Gulf of Guayaquil (Ecuador) during the Quaternary as an effect of the North Andean block tectonic escape. Tectonics 25, TC3017. https://doi.org/10.1029/2004TC001723.
Yepes, H., Audin, L., Alvarado, A., Beauval, C., Aguilar, J., Font, Y., Cotton, F., 2016. A new view for the geodynamics of Ecuador: Implication in seismogenic source definition and seismic hazard assessment. Tectonics 35, 1249–1279. https://doi.org/10.1002/2015TC003941.